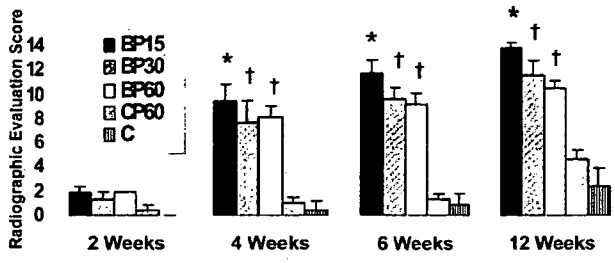

Fig 4. Radiographic evaluation score was measured at each period after surgery. Ten animals at 2 weeks, eight at 4 weeks, seven at 6 weeks, and five at 12 weeks were assigned to each group postoperatively. The bar represents mean ± standard deviation. * = $p < 0.01$ (compared with all other groups); † = $p < 0.01$ (compared with the C and CP60 groups). The scores in all BP groups were substantially higher than those of the control animals (the CP60 and C groups) at 4, 6, and 12 weeks.

As assessed using manual testing of the samples harvested at 12 weeks, all of the femurs from the three BP groups were estimated to have successful consolidation, whereas those from the control animals had failed consolidation (Table 3). The mean values of maximum strength of the reimplanted femurs as assessed on the three-point bending tests indicated that the three BP groups were stronger ($p < 0.01$) than those from the control groups (Fig 7). Among the three BP groups, the maximum strength was higher ($p < 0.01$) in the BP15 group despite less callus formation than in the other two groups.

DISCUSSION

We assessed a method of reconstructing rat femoral defects using reimplantation of the devitalized, resected segments coated with rhBMP-2 in a biodegradable carrier. The results suggest reimplantation of extracorporeally devitalized autogenous bone segments predictably repair critical-sized rat femoral defect when combined with a rhBMP-2-containing resorbable paste. This method potentially could be used to reconstruct defects frequently encountered during limb salvage surgery for treatment of musculoskeletal malignancies. When considering the practical application of this repair method in conjunction with the devitalized tumor-bearing bone, the dose of rhBMP-2 should be reconsidered because the minimal essential dose of rhBMP-2 is different depending on the recipient species.[34] In highly evolved animals or humans, the responsiveness to rhBMP-2 is much lower than in rodents. The dose of rhBMP-2 per square centimeter of devitalized bone surface was 1.4 μg in our study. If the responsiveness of humans is 20 times lower than that of rats, the essential dose in humans may be closer to 28 $\mu g/cm^2$. Also, as a previous study indicated,[17] responsiveness to rhBMP-2 is age-dependent. Therefore, additional preclinical experiments in a large animal model and/or in primates and, ultimately, clinical trials will be required to optimize the dose of rhBMP-2.

The reimplantation of a devitalized, autogenous bone segment was first reported by Galle in 1918 with use of

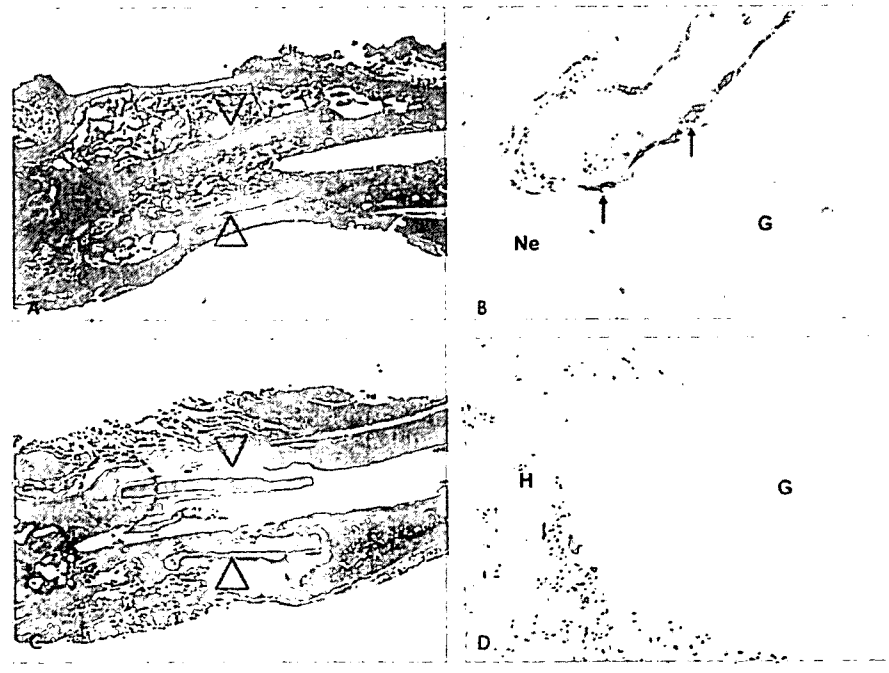

Fig 5A–D. Histologic sections prepared from (A, B) the BP15 group and (C, D) the C group at 4 weeks after surgery are shown (A, C: stain, hematoxylin and eosin; original magnification, ×40; B, D: higher-magnified views from the circled areas; stain, TRAP; original magnification, ×200). Ne = newly formed bone; G = reimplanted bone; H = host bone. Arrowheads indicate the implanted autoclaved bone segment and arrows indicate TRAP-positive cells or osteoclasts on the surface of the autoclaved bone. The reimplanted bone segment was encased in the newly formed bone with marrow and the autoclaved bone was incorporated into the repaired bone in the BP15 group. The reimplanted bone was not repaired by new bone formation in the C group.

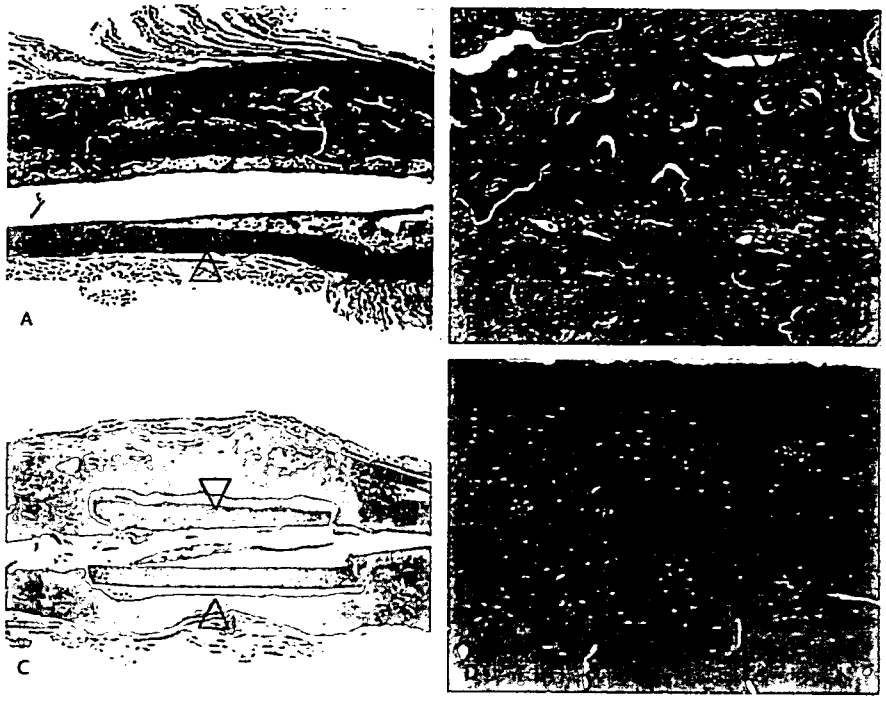

Fig 6A–D. Histologic sections prepared from (A, B) the BP15 group and (C, D) the C group at 12 weeks after surgery are shown (A, C: stain, hematoxylin and eosin; original magnification, ×40; B, D: longitudinal sections of cortical bone of autoclaved segments; stain, hematoxylin and eosin; original magnification, ×200). The reimplanted bone segment is partially resorbed and replaced with new bone (arrowheads) in the BP15 group. The reimplanted bone was embedded in fibrous tissue and remodeling activity was not seen in the C group.

boiled tumor-bearing bone mass. Since then, numerous similar reports have been published, and the reimplantation of devitalized tumor-bearing bone segments have been an option for reconstruction of bone defects generated by wide resection of malignant bone tumors, especially when the resected bone has enough strength to support the mechanical loads applied to the affected bone. Although the reimplanted bone tissue offers advantages in terms of being able to match the size of the defect, a low risk for local tumor recurrence, avoidance of immune reactions, and low cost, the clinical results have been disappointing as a result of delayed or nonunion of the reimplanted bone and gradual resorption of the reimplanted graft leading to mechanical weakness and fracture. These disadvantages appear to result from the lack of the osteogenic potential of the reimplanted bone devitalized by autoclaving, pasteurization, or radiation.[3,30] Restoration of the osteogenic potential of the reimplanted bone should improve the clinical results without loss of the advantages described. This prompted us to look at the possibility of overcoming these problems by combining rhBMP-2 and its delivery system with the devitalized resected bone.

In the rat bone defect model used in our study, rhBMP-2 was used because of its known biologic efficacy

TABLE 3. Union Rates Assessed by Radiography and Manual Palpation

Group	Number of Unions by Radiography	Number of Unions by Manual Palpation
BP60	5/5	5/5
BP30	5/5	5/5
BP15	5/5	5/5
CP60	2/5	0/5
C	0/5	0/5

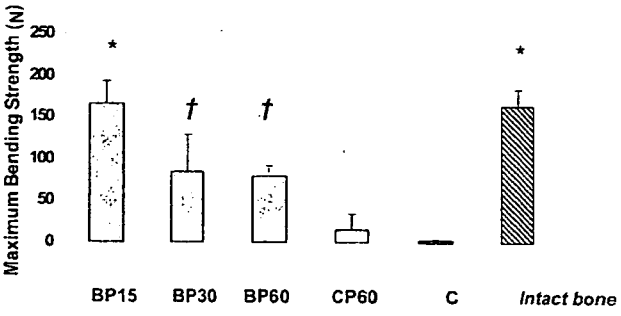

Fig 7. Reimplanted femurs harvested 12 weeks postoperatively were subjected to a three-point bending test. The bar represents mean ± standard deviation (n = 5). * = $p < 0.01$ (compared with the BP30, BP60, CP60, and C groups); † = $p < 0.01$ (compared with the CP60 and C groups). Among the three BP groups, the maximum strength was substantially higher in the BP15 group.

in nonhuman species.[13,22,25] Clinical use of rhBMP-2 has been approved by the FDA and often is used in combination with a biodegradable bovine collagen carrier for spinal fusion surgery in the United States.[4,8] In our study, a synthetic biodegradable block copolymer (PLA-PEG) was developed to serve as an alternative biodegradable carrier for rhBMP-2.[10,26,27] This synthetic biodegradable polymer and β-TCP powder were used instead of collagen.[18] Adding the β-TCP powder in an amount equal to the polymer modifies the sticky gel-like nature of the PLA-PEG at room temperature to create a less sticky dough that was coated on the surface of the devitalized bone segments. As expected, the dough or paste implant was resorbed and new bone was formed, probably through the sustained release of the rhBMP-2 from the degrading paste.

Although we noted a correlation between the amount of rhBMP-2-retaining paste and newly formed bone mass around the reimplanted bone segments on radiographs at times longer than 4 weeks after reimplantation, the mechanical strength of the repaired femurs at 12 weeks did not correlate with the new bone mass around the devitalized bone segments. Unexpectedly, the femur that received 15 mg of paste and yielded the smallest amount of callus most effectively restored the strength of the intact femur at 12 weeks. Devitalized bone segments that received larger amounts of the rhBMP-2-containing dough (BP60 and BP30 femurs) did not show a more rapid recovery in bone strength. Thus, the optimal amount of dough in our model was 15 mg, representing an optimal rhBMP-2 dose of approximately 2.5 μg. A possible explanation might be that the higher doses of rhBMP-2 led to a dose-dependent larger callus with a mechanically weaker structure at the periphery, resulting in comparative weakness on the three-point bending test. Radiographic and histologic features in the BP15 group indicated a more complete remodeling of the callus resulting in a thicker cortex with greater strength. These features might be the consequence of an accelerated remodeling of the callus at this optimal rhBMP-2 dose. Despite larger calluses in BP30 and BP60 samples, a thinner cortical shell resulting from inadequate remodeling might have resulted in the weakness, suggesting further time for remodeling to achieve comparable mechanical strength is needed at higher rhBMP-2 doses. Another possible explanation is that this is the result of an increased rate of bone resorption in the presence of higher doses of rhBMP-2, as described in previous reports.[19] In fact, histologic examination at 12 weeks showed there was less trabecular bone inside the shell-like calluses in the BP60 groups.

The findings of this experimental study suggest this reimplantation method with the use of rhBMP-2 represents a new approach for reconstruction of bone defects resulting from wide resection of tumors in the extremities or trunk and offers an alternative to implantation of a prosthesis or the use of vascularized or nonvascularized bone grafting.

Acknowledgments

We thank Masatoshi Hoshino, MD, and Masahiro Yoneda, MD, Department of Orthopedic Surgery, Graduate School of Medicine, Osaka City University, for advice and expertise.

References

1. Ahmed AR, Manabe J, Kawaguchi N, Matsumoto S, Matsushita Y. Radiographic analysis of pasteurized autologous bone graft. *Skeletal Radiol.* 2003;32:454–461.
2. Araki N, Myoui A, Kuratsu S, Hashimoto N, Inoue T, Kudawara I, Ueda T, Yoshikawa H, Masaki N, Uchida A. Intraoperative extracorporeal autogenous irradiated bone grafts in tumor surgery. *Clin Orthop Relat Res.* 1999;368:196–206.
3. Asada N, Tsuchiya H, Kitaoka K, Mori Y, Tomita K. Massive autoclaved allografts and autografts for limb salvage surgery: a 1–8 year follow-up of 23 patients. *Acta Orthop Scand.* 1997;68: 392–395.
4. Boden SD, Kang J, Sandhu H, Heller JG. Use of recombinant human bone morphogenetic protein-2 to achieve posterolateral lumbar spine fusion in humans: a prospective, randomized clinical pilot trial: 2002 Volvo Award in clinical studies. *Spine.* 2002;27: 2662–2673.
5. Bohm P, Fritz J, Thiede S, Budach W. Reimplantation of extracorporeal irradiated bone segments in musculoskeletal tumor surgery: clinical experience in eight patients and review of the literature. *Langenbecks Arch Surg.* 2003;387:355–365.
6. Bohm P, Springfeld R, Springer H. Re-implantation of autoclaved bone segments in musculoskeletal tumor surgery: clinical experience in 9 patients followed for 1.1–8.4 years and review of the literature. *Arch Orthop Trauma Surg.* 1998;118:57–65.
7. Bohm P, Stihler J. Intraosseous temperature during autoclaving. *J Bone Joint Surg Br.* 1995;77:649–653.
8. Burkus JK, Sandhu HS, Gornet MF, Longley MC. Use of rhBMP-2 in combination with structural cortical allografts: clinical and radiographic outcomes in anterior lumbar spinal surgery. *J Bone Joint Surg Am.* 2005;87:1205–1212.
9. Enneking WF, Campanacci DA. Retrieved human allografts: a clinicopathological study. *J Bone Joint Surg Am.* 2001;83:971–986.
10. Kato M, Toyoda H, Namikawa T, Hoshino M, Terai H, Miyamoto S, Takaoka K. Optimized use of a biodegradable polymer as a carrier material for the local delivery of recombinant human bone morphogenetic protein-2. *Biomaterials.* 2006;27:2035–2041.
11. Khattak MJ, Umer M. Haroon-ur-Rasheed, Umar M. Autoclaved tumor bone for reconstruction. *Clin Orthop Relat Res.* 2006;447: 138–144.
12. Kotz R, Ritschl P, Trachtenbrodt J. A modular femur-tibia reconstruction system. *Orthopedics.* 1986;9:1639–1652.
13. Lee FY, Storer S, Hazan EJ, Gebhardt MC, Mankin HJ. Repair of bone allograft fracture using bone morphogenetic protein-2. *Clin Orthop Relat Res.* 2002;397:119–126.
14. Manabe J, Ahmed AR, Kawaguchi N, Matsumoto S, Kuroda H. Pasteurized autologous bone graft in surgery for bone and soft tissue sarcoma. *Clin Orthop Relat Res.* 2004;419:258–266.
15. Mankin HJ, Gebhardt MC, Jennings LC, Springfield DS, Tomford WW. Long-term results of allograft replacement in the management of bone tumors. *Clin Orthop Relat Res.* 1996;324:86–97.
16. Mankin HJ, Hornicek FJ, Raskin KA. Infection in massive bone allografts. *Clin Orthop Relat Res.* 2005;432:210–216.
17. Matsumoto A, Yamaji K, Kawanami M, Kato H. Effect of aging on bone formation induced by recombinant human bone morphogenetic protein-2 combined with fibrous collagen membranes at subperiosteal sites. *J Periodontal Res.* 2001;36:175–178.

18. Matsushita N, Terai H, Okada T, Nozaki K, Inoue H, Miyamoto S, Takaoka K. A new bone-inducing biodegradable porous beta-tricalcium phosphate. *J Biomed Mater Res A.* 2004;70: 450–458.
19. McClellan JW, Mulconrey DS, Forbes RJ, Fullmer N. Vertebral bone resorption after transforaminal lumbar interbody fusion with bone morphogenetic protein (rhBMP-2). *J Spinal Disord Tech.* 2006;19:483–486.
20. Mittermayer F, Krepler P, Dominkus M, Schwameis E, Sluga M, Heinzl H, Kotz R. Long-term followup of uncemented tumor endoprostheses for the lower extremity. *Clin Orthop Relat Res.* 2001; 388:167–177.
21. Murakami N, Saito N, Takahashi J, Ota H, Horiuchi H, Nawata M, Okada T, Nozaki K, Takaoka K. Repair of a proximal femoral bone defect in dogs using a porous surfaced prosthesis in combination with recombinant BMP-2 and a synthetic polymer carrier. *Biomaterials.* 2003;24:2153–2159.
22. Murnaghan M, McIlmurray L, Mushipe MT, Li G. Time for treating bone fracture using rhBMP-2: a randomised placebo controlled mouse fracture trial. *J Orthop Res.* 2005;23:625–631.
23. Namikawa T, Terai H, Suzuki E, Hoshino M, Toyoda H, Nakamura H, Miyamoto S, Takahashi N, Ninomiya T, Takaoka K. Experimental spinal fusion with recombinant human bone morphogenetic protein-2 delivered by a synthetic polymer and beta-tricalcium phosphate in a rabbit model. *Spine.* 2005;30:1717–1722.
24. Ozaki T, Hillmann A, Wuisman P, Winkelmann W. Reconstruction of tibia by ipsilateral vascularized fibula and allograft: 12 cases with malignant bone tumors. *Acta Orthop Scand.* 1997;68: 298–301.
25. Pluhar GE, Manley PA, Heiner JP, Vanderby R, Seeherman HJ, Markel MD. The effect of recombinant human bone morphogenetic protein-2 on femoral reconstruction with an intercalary allograft in a dog model. *J Orthop Res.* 2001;19:308–317.
26. Saito N, Okada T, Horiuchi H, Murakami N, Takahashi J, Nawata M, Ota H, Nozaki K, Takaoka K. A biodegradable polymer as a cytokine delivery system for inducing bone formation. *Nat Biotechnol.* 2001;19:332–335.
27. Saito N, Takaoka K. New synthetic biodegradable polymers as BMP carriers for bone tissue engineering. *Biomaterials.* 2003;24: 2287–2293.
28. Sakayama K, Kidani T, Fujibuchi T, Kamogawa J, Yamamoto H, Shibata T. Reconstruction surgery for patients with musculoskeletal tumor, using a pasteurized autogenous bone graft. *Int J Clin Oncol.* 2004;9:167–173.
29. Sugiura H, Yamamura S, Sato K, Katagiri H, Nishida Y, Nakashima H, Yamada Y. Remodelling and healing process of moderately heat-treated bone grafts after wide resection of bone and soft-tissue tumors. *Arch Orthop Trauma Surg.* 2003;123:514–520.
30. Suk KS, Shin KH, Hahn SB. Limb salvage using original low heat-treated tumor-bearing bone. *Clin Orthop Relat Res.* 2002;397: 385–393.
31. Takami H, Takahashi S, Ando M, Masuda A. Vascularized fibular grafts for the reconstruction of segmental tibial bone defects. *Arch Orthop Trauma Surg.* 1997;116:404–407.
32. Torbert JT, Fox EJ, Hosalkar HS, Ogilvie CM, Lackman RD. Endoprosthetic reconstructions. *Clin Orthop Relat Res.* 2005;438: 51–59.
33. Urist MR, Strates BS. Bone morphogenic protein. *J Dent Res.* 1971; 50:1392–1406.
34. Valentin-Opran A, Wozney J, Csimma C, Lilly L, Riedel GE. Clinical evaluation of recombinant human bone morphogenetic protein-2. *Clin Orthop Relat Res.* 2002;395:110–120.
35. Wang J, Temple HT, Pitcher JD, Mounasamy V, Malinin TI, Scully SP. Salvage of failed massive allograft reconstruction with endoprosthesis. *Clin Orthop Relat Res.* 2006;443:296–301.
36. Wheeler DL, Enneking WF. Allograft bone decreases in strength in vivo over time. *Clin Orthop Relat Res.* 2005;435:36–42.
37. Yuehuei H. Animal models of bone defect repair. In: Yuehuei HA, Richard JF, eds. *Animal Models in Orthopaedic Research.* Boca Raton, FL: CRC Press; 1999:241–260.

Regenerative Repair of Long Intercalated Rib Defects Using Porous Cylinders of β-Tricalcium Phosphate: An Experimental Study in a Canine Model

Masatoshi Hoshino, M.D.
Takeshi Egi, M.D.
Hidetomi Terai, Ph.D.
Takashi Namikawa, M.D.
Kunio Takaoka, Ph.D.
Osaka, Japan

Background: In maxillofacial, spinal, and orthopedic surgery, bony ribs have been used as a source of donor bone. The resultant defects are not usually repaired, despite the pain or cosmetic morbidity experienced by the patient. The authors evaluated the efficacy of an osteoconductive β-tricalcium phosphate and the contribution of the periosteum in rib bone regeneration.
Methods: Two 8-cm-long intercalated rib defects were generated in each of 30 beagle dogs. In the first group ($n = 15$), one defect was implanted with 16 small, short, porous β-tricalcium phosphate cylinders that were connected with a titanium wire, and the other defect was left untreated. In the remaining 15 dogs, the periosteum was devitalized by ethanol, and then the same surgical procedures were performed. Each group was subdivided into three groups ($n = 5$), and the animals were euthanized at 3, 6, and 12 weeks. Bone regeneration was assessed radiologically, histologically, and mechanically.
Results: In the defect implanted with β-tricalcium phosphate on intact periosteum, newly formed bone was present on and in the β-tricalcium phosphate cylinders and bridged both ends of the resected ribs at 12 weeks, with replacement of β-tricalcium phosphate by new bone. Mechanical testing of these ribs revealed that they had 70 percent of the strength of normal ribs when compared in a bending stress test at 12 weeks after surgery. No regenerative bone bridging the rib defects was seen in the ethanol-devitalized or untreated groups.
Conclusions: Porous β-tricalcium phosphate cylinders placed in tandem on the intact periosteum might be useful for the repair of rib bone donated at surgery, presenting a new and unique method for regenerating rib defects. (*Plast. Reconstr. Surg.* 119: 1431, 2007.)

In maxillofacial, spinal, and orthopedic surgery, bone from ribs, ilium, and fibula has served as donor material to repair bone defects and to promote spinal fusion because of its superior osteogenic potential and acceptable clinical results.[1,2] However, the defects in the donor ribs are currently left unrepaired despite donor-site pain and cosmetic morbidity.[3,4] This issue has not been addressed in part because of the limited impact on respiratory function and/or lack of effective methods for regenerating the lost rib. In limited cases, various rib prostheses have been used to preserve respiratory function.[5,6] However, concerns regarding infection and limited clinical results remain because of limited biocompatibility and osteogenic potential of the prosthesis to regenerate the rib.

For bone substitutes, ceramic implants such as hydroxyapatite and tricalcium phosphate have been investigated extensively because of their good biocompatibility and osteoconductive properties. These have been used clinically and have shown acceptable surgery-related results.[7,8] Hydroxyapatite has the advantage of mechanical strength, but has the disadvantage of a long residence time. β-Tricalcium phosphate is degraded with the help of osteoclasts and replaced by new bone when incorporated into osseous tissue.[9,10] Recently, highly pure porous β-tricalcium phosphate has been manufactured using a mechanochemical method.

From the Department of Orthopedic Surgery, Osaka City University Graduate School of Medicine.
Received for publication July 20, 2005; accepted September 28, 2005.

DOI: 10.1097/01.prs.0000256319.89619.c8

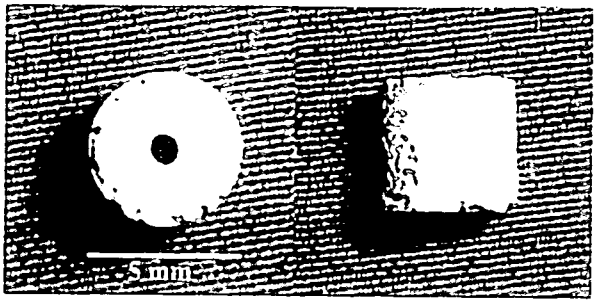

Fig. 1. Macroscopic aspect of the β-tricalcium phosphate cylinder. The cylinder has an outer diameter 5 mm, an inner diameter of 1 mm, and a height of 5 mm.

Porous β-tricalcium phosphate possessing macropores of 100 to 500 μm and micropores of less than 5 μm is now available as a degradable implant. In this material, almost all the macropores are interconnected by means of 100- to 200-μm paths. These structures facilitate the infiltration of osteogenic cells. The effective bioabsorbability and osteoconductivity of this β-tricalcium phosphate have been documented in both animal experiments and clinical studies.[11–15]

To improve the methods for regenerating ribs or to preserve respiratory function resulting from rib bone loss, we attempted to produce a new implant material using β-tricalcium phosphate. The implants were fabricated into short cylindrical blocks and connected in tandem with titanium wire passed through the cylinders.

The presence or absence of intact periosteum at the rib defect might influence the regeneration potential because of the osteogenic capacity of the periosteum. In clinical cases such as defects in donor sites after vascularized rib grafting or by excision of malignant or benign tumors originated from ribs or soft tissue of the thoracic cage, the rib defects should be repaired under the condition without intact periosteum. Thus, a rib defect model with periosteum devitalized by contact with ethanol was also made to examine the contribution of the periosteum to rib defect repair in this study. The purpose of this study was to evaluate the efficacy of small cylinders of an osteoconductive biomaterial, β-tricalcium phosphate, and the contribution of the periosteum in rib bone regeneration.

MATERIALS AND METHODS

Preparation of Porous β-Tricalcium Phosphate

β-Tricalcium phosphate powder was synthesized by wet milling (a mechanochemical method). The preparation of this material involves milling dicalcium phosphate dihydrate and calcium carbonate at a molar ratio of 2:1 with pure water and zirconium beads, followed by drying at 80°C. The resultant crystalline solid is converted to β-tricalcium phosphate by calcinations at 750°C for 1 hour. On sintering of the β-tricalcium phosphate powder at 1050°C for 1 hour, a porous β-tricalcium phosphate block was created, which was then characterized in terms of surface area and pore size distribution. The porosity of the block, as measured by the Archimedes method, was 75 percent. The β-tricalcium phosphate block possesses macropores of 100 to 500 μm and micropores of less than 5 μm. Nearly all macropores are interconnected. The porous β-tricalcium phosphate was cut into cylinders (outer diameter, 5 mm; inner diameter, 1 mm; height, 5 mm) with an average weight of 70 mg, and provided to us as a sterile material by Olympus Biomaterial Co., Ltd. (Tokyo, Japan) for this study (Fig. 1).

Preparation of Composite Implants

To assemble a composite implant, a curved titanium wire 0.8 mm in diameter and 12 cm in length was passed through the 15 or 16 β-tricalcium phosphate cylinders under sterile conditions (Fig. 2).

Experimental Animals

Thirty male beagle dogs, 8 months old, with an average body weight of 10 kg (range, 9.5 to 10.5

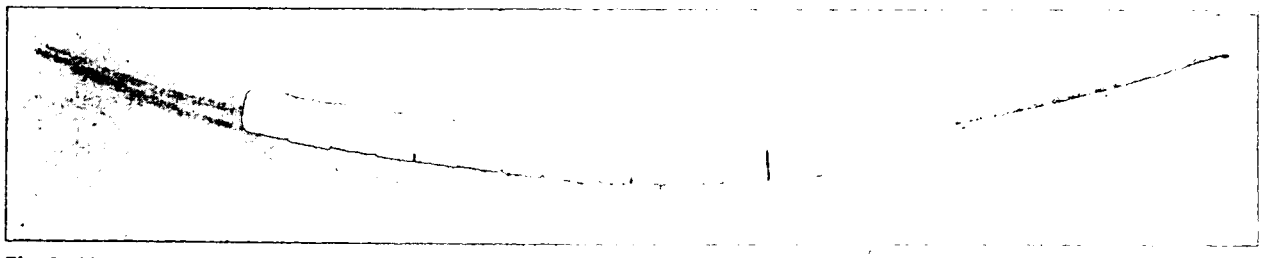

Fig. 2. Macroscopic aspect of the β-tricalcium phosphate cylinder. Sixteen cylinders are connected by passing a titanium wire (0.8 mm in diameter) through each cylinder.

kg) were purchased from Oriental Yeast Co. (Tokyo, Japan), and housed in separate cages with free access to food and water.

Surgical Procedures

Each animal was anesthetized by means of an intramuscular injection of ketamine (10 mg/kg) and xylazine (1.2 mg/kg) and maintained under anesthesia with an intravenous injection of pentobarbital (25 mg/kg). Cephazolin (10 mg/kg) was administered subcutaneously as a prophylactic antibiotic. After intratracheal intubation, the animal was placed in the right lateral position on an operating table, and skin hair over the left thoracic cage was removed with a hair cutter. The skin was sterilized with povidone-iodine solution and wrapped using sterile technique. In 15 dogs, a skin incision 10 cm long on and along the left tenth rib was made, and the outer surface of the thoracic cage was exposed. The tenth ribs, 8 cm long, were removed together with periosteum on the outer surfaces of the ribs. The periosteum on the inner wall of the ribs remained on the thoracic cage. The assembled prosthesis was placed into the defects in the tenth rib (tricalcium phosphate group) (Table 1). The implanted prosthesis was fixed to the cut ends of the ribs by intramedullary insertion of the titanium wires. The end of the wires was pushed out of the cortical bone of the rib through a drill hole to facilitate removal at 6 weeks after surgery (Fig. 3). The intercostal muscles were brought into contact with the implants by rough sutures and skin with close interrupted sutures. By the same surgical procedures through an additional skin incision along the fourth rib, the defect in this rib did not receive any implants (defect group). In another group of 15 dogs, the inner periosteum of the tenth rib defects was treated with 99% ethanol to devitalize the osteogenic cells on the cambium layer of the periosteum. Then, the prosthesis was placed (tricalcium phosphate/ethanol group). In addition, the inner periosteum in the fourth rib defect with no implant received similar alcohol treatment (defect/ethanol group). Table 1 summarizes the surgical procedures for each rib group. After surgery, all the animals were monitored closely and had ad libitum access to food and water for 12 weeks. The experimental protocol was approval by the Institutional Committee for Animal Care and Experiments of Osaka City University Graduate School of Medicine and performed under strict accordance with appropriate guidelines.

Table 1. Surgical Procedures for Each Group*

	β-TCP	
	Negative	Positive
ETOH		
Negative	Defect	TCP
Positive	Defect/ETOH	TCP/ETOH

β-TCP, the defect was implanted with 16 small short porous β-tricalcium phosphate cylinders; ETOH, the periosteum of rib defect was devitalized by 99% ethanol.
*These groups were each subdivided into three groups ($n = 5$), and the animals were euthanized at 3, 6, and 12 weeks.

Sample Preparation

These two groups were each subdivided into three groups ($n = 5$), and the animals were euthanized by means of an overdose of anesthetics at 3, 6, and 12 weeks. At each of these time points, the fourth and tenth ribs, including defects, were dissected free. The seventh ribs were removed from dogs that had not been operated on for use as normal controls. All dissected samples were radiographed and fixed in 10% neutral buffered formalin. The rib specimens were examined for evidence of new bone formation by the use of radiographic, histologic, and biomechanical methods.

Radiographic Examinations

Plain radiographs of the removed ribs were taken by means of routine procedures. The samples were cut to 3-mm thickness perpendicular to the rib axis at the middle of the original defects and radiographs were obtained. These radiographic images were examined for changes in radiographic densities in and around the implants at the rib defects.

Mechanical Testing

The tricalcium phosphate group and the tricalcium phosphate/ethanol group ribs retrieved from chest walls at 3, 6, and 12 weeks after surgery were subjected to mechanical testing by three-point bending using an apparatus designed for this purpose (Maruto Testing Machine Co., Tokyo, Japan). The stiffness of the defect segment was measured on a stress/deformity curve. The stiffness of normal ribs was measured as normal controls.

Histology

After the radiographic and biomechanical examinations, undecalcified histologic sections of the rib defects were prepared. The rib samples

Fig. 3. Intraoperative view of β-tricalcium phosphate cylinders placed in the defect of the rib. The ends of the titanium wire were placed into the medullary canal of both ends of the original rib and passed through the outer cortices of the rib to fix the implant. This also enabled the removal of the titanium wire after repair of the rib defect.

fixed in neutral buffered formalin were dehydrated in gradient ethanol and embedded in polymerized methylmethacrylate and cut to 10-μm thickness perpendicular to the rib axis at the middle of the original defects and stained by means of the Villanueva bone staining method. In addition, a histochemical method to detect tartrate-resistant acid phosphatase, an enzyme specific to osteoclast, was used. Briefly, the paraffin-removed sections were placed in the tartrate-resistant acid phosphatase staining solution consisting of acetate buffer (pH 5.0) containing 50 mM sodium tartrate, 25 mg/ml naphthol-ASMX phosphate (Sigma Chemical Co., St. Louis, Mo.), and 0.5 mg/ml fast red violet salt (Sigma). The sections were incubated with the solution at 37°C for 20 minutes. After washing, the sections were counterstained with methyl green and observed under a light microscope.

Statistical Analysis

The quantitative values obtained from measurement of stiffness were expressed as means ± SD and compared using the Kruskal-Wallis test. Differences between experimental groups were evaluated with the post hoc Tukey-Kramer test. Differences at $p < 0.05$ were considered significant.

RESULTS

Gross Inspection and Palpation Test

All 30 dogs underwent surgery successfully and survived without any difficulty during the 12 postoperative weeks. No abnormality relating to surgical-site infection was noted. The respiratory movement of the chest wall with the prosthetic implants was normal, without paradoxical movement when inspected just before the animals were euthanized. On inspection of the surface of the harvested chest cages at 3 weeks postoperatively, the cylinder implants placed in defects in the tricalcium phosphate group and the tricalcium phosphate/ethanol group ribs were identical and the tandem arrangement of β-tricalcium phosphate cylinders was recognized in the rib defects. In the defect group ribs and the defect/ethanol group ribs, the defects were filled with a fibrous tissue mass. At 6 weeks after surgery, the rib defects in the tricalcium phosphate group were harder than those from other control defects, but there was no significant difference in gross appearance of the defects of other respective group rib samples compared with those harvested 3 weeks after surgery. At 12 weeks after surgery, the rib defects in the entire tricalcium phosphate group were covered with hard tissue that bridged both ends of the rib defects and restored mechanical stiffness on palpation. In the defects in the tricalcium phosphate/ethanol group ribs, no evidence of hard tissue adjacent to the β-tricalcium phosphate cylinder implants or mechanical stiffness was found. In the defect group ribs, a thin layer of hard tissue mass with connection to the rib ends was found in the defects on palpation. In the defect/ethanol group, there was no evidence of palpable hard tissue mass.

Radiographic Examinations

In the tricalcium phosphate group ribs, on plain radiographs of the rib defects harvested at 12 weeks after surgery, a radiopaque shadow or new bone was consistently noted on and between the

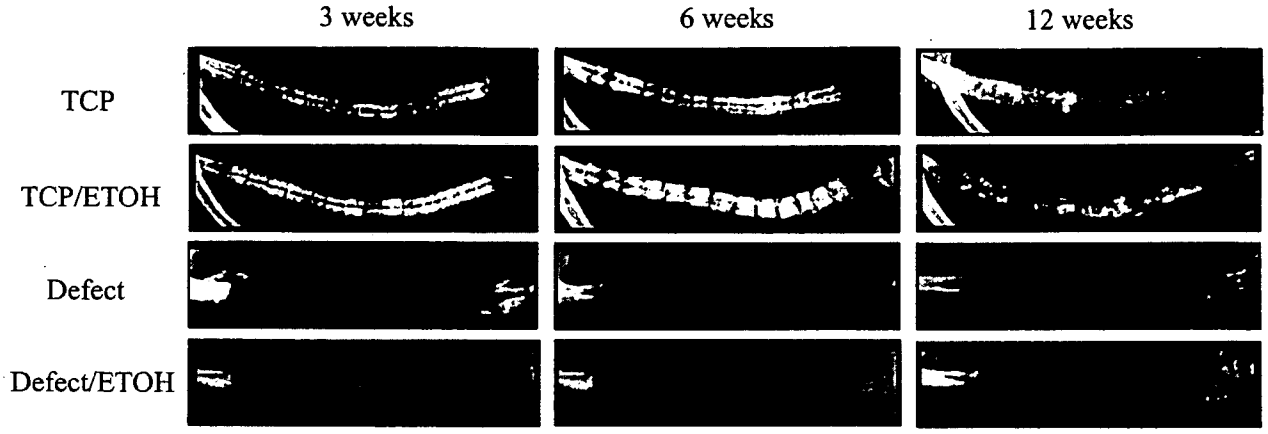

Fig. 4. Representative plain radiographs of the ribs (*above*) implanted with β-tricalcium phosphate. (*Second row*) β-Tricalcium phosphate with alcohol treatment of the periosteum; (*third row*) control defects with no implants; and (*below*) defects with no implants and alcohol treatment of the periosteum. Sequential radiographs show bone repair at 3, 6, and 12 weeks after implantation in the tricalcium phosphate group.

series of the β-tricalcium phosphate cylinders and connected to both ends of the original rib in four of five samples (Fig. 4). In one of five, new bone was noted over almost the entire defect but not connected completely. The radiopaque shadows were noted predominantly on the inner surface of the β-tricalcium phosphate cylinders at 3 weeks after surgery (Fig. 5). These shadows were not noted in defects in the tricalcium phosphate/ethanol group ribs. The respective β-tricalcium phosphate cylinder encased within the new bone in the tricalcium phosphate group was significantly reduced from its original size over the 12-week test period. The size reduction was also seen in the tricalcium phosphate/ethanol group ribs but to a lesser degree when compared with that in the tricalcium phosphate group. In all defect group ribs, radiopaque shadows in the defects that were connected from cut ends of the ribs were observed. In the defect/ethanol group, these radiopaque shadows were absent over the experimental period of 12 weeks. Table 2 shows the incidence of bone defect repair on radiographic assessments.

Mechanical Testing

The stiffness of the tricalcium phosphate group ribs started to increase 6 weeks after surgery and reached 70 percent of that found in a normal rib at 12 weeks. The tricalcium phosphate/ethanol group ribs had much less stiffness than the tricalcium phosphate group ribs. The stiffness of the tricalcium phosphate and tricalcium phosphate/ethanol group ribs at 3 and 6 weeks and of the tricalcium phosphate/ethanol group ribs at 12 weeks was significantly lower than that of normal ribs at the same time points (Fig. 6).

Histology

On undecalcified cross-sections of the midportion of the defect in the tricalcium phosphate group harvested at 3 weeks, a thin layer of new bone in contact with the inner surface of the cylinder was observed (Fig. 7). At both ends of the defect in the tricalcium phosphate group, the new bone united the preexisting rib bone and the regenerated rib. Multinucleated giant cells were located in the new bone predominantly on the surface of the porous β-tricalcium phosphate implant at the midportion. Those cells revealed an osteoclastic phenotype based on the tartrate-resistant acid phosphatase–positive histochemical staining (Fig. 8). In contrast, in the tricalcium phosphate/ethanol group, no apparent bone formation was noted and fibrous tissue layers were seen on the surface of the implants. A small mass of new bone was seen at the cut ends of the ribs, where tartrate-resistant acid phosphatase–positive multinucleated cells were sparsely distributed on the surface of the β-tricalcium phosphate implant. On sections of the 6-week samples of the tricalcium phosphate group ribs, new bone growth with hematopoietic marrow was seen on and in the porous β-tricalcium phosphate implants. On sections of the defect group ribs, a thin layer of bone mass at the cut ends of the ribs was noted. On cross-sections of the 12-week samples of the tricalcium phosphate group, the β-tricalcium phosphate implant was almost completely resorbed, presumably because of continuous resorption of the implant

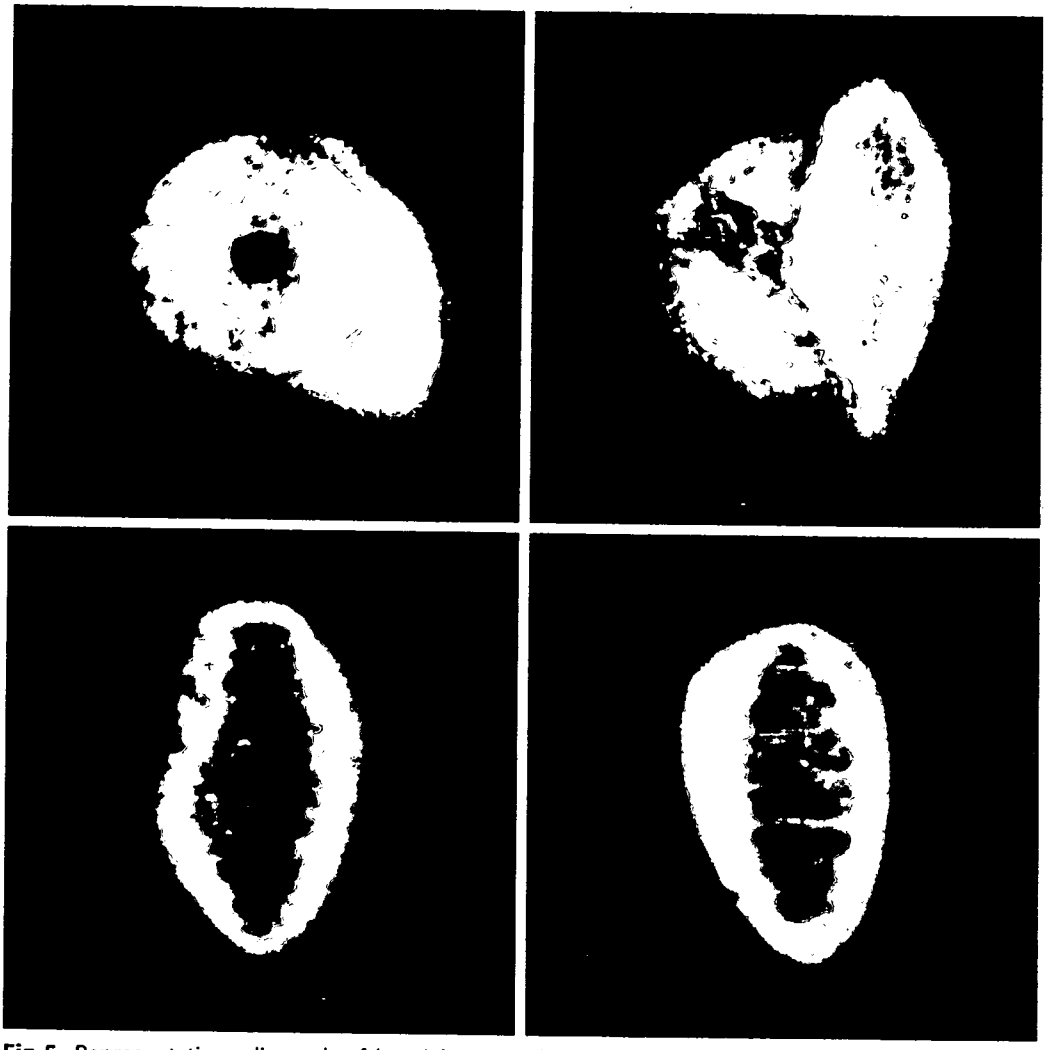

Fig. 5. Representative radiographs of the axial section of the midportion of the defects. Tricalcium phosphate group at 3 weeks (*above, left*), 6 weeks (*above, right*), and 12 weeks (*below, left*). Normal rib (*below, right*). The radiopaque shadows were noted on the inner surface of the β-tricalcium phosphate cylinders. The respective β-tricalcium phosphate cylinder encased within the new bone was significantly reduced from its original size. Regenerative repair with restoration of anatomical configuration was achieved.

by the large population of tartrate-resistant acid phosphatase–positive osteoclastic cells (Fig. 7). In sections from tissues retrieved from animals in the tricalcium phosphate/ethanol group, the implants remained nonresorbed without new bone formation. In the defect group, small bone masses were formed on the periosteum, but these were of insufficient volume to repair the rib defects or unite with the rib ends. In the defect/ethanol group, no new bone was recognized on histologic examination.

Table 2. Incidence of Rib Defect Repair on Radiographic Assessments

Group of Ribs	3 Weeks	6 Weeks	12 Weeks
TCP	0/5	1/5	4/5
TCP/ETOH	0/5	0/5	0/5
Defect	0/5	0/5	0/5
Defect/ETOH	0/5	0/5	0/5

TCP, tricalcium phosphate; ETOH, ethanol.

DISCUSSION

The results presented in this study show successful and reproducible regenerative repair of intercalated rib defects of critical size (8 cm) through the use of biocompatible, osteoconductive, and degradable porous β-tricalcium phosphate placed on the intact periosteum in dogs.

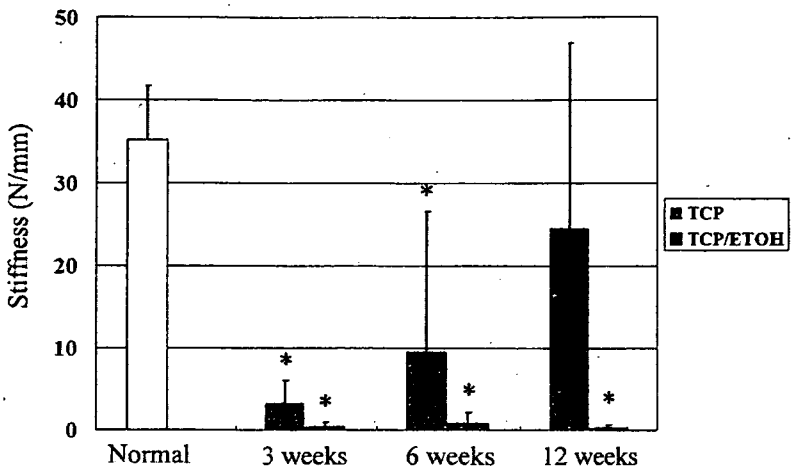

Fig. 6. The results of the three-point bending test of the defects in the tricalcium phosphate group, the tricalcium phosphate/ethanol group, and the normal control ribs at 3, 6, and 12 weeks after surgery are shown. The stiffness of the tricalcium phosphate group at 12 weeks reached a value corresponding to 70 percent of a normal rib. *Statistically significant difference from a normal rib.

The rib defects that did not receive implants were not repaired in 12 weeks, thus confirming the belief that the defect size adopted in this experimental study had exceeded the natural regenerating potential in dogs.

The successful regeneration of the rib defects might have been caused by the osteogenic potential of the periosteum of the ribs remaining on the chest wall, because alcohol treatment of the periosteal surface and the resultant devitalization of the osteogenic cells eliminated the regenerating reaction.[16,17] Another possible reason for the successful repair could have been the use of osteoconductive porous β-tricalcium phosphate cylinders in combination with titanium wires to accommodate the anatomical curvature of the rib. The inherent flexibility of this implant was likely permissive to the reciprocating microdeformities caused by respiratory movements of the chest cage. As a result, there was no displacement or breakage of the brittle β-tricalcium phosphate cylinders or fixation to the ribs. In an osteoinductive environment with intact periosteum, β-tricalcium phosphate might be useful for the repair of load-bearing skeletal defects, even in long bones. However, because β-tricalcium phosphate is brittle under mechanical loading, internal or external fixation should be used to avoid collapse of β-tricalcium phosphate blocks in such situation. The porous structure of the implants was beneficial for bone growth into the biomaterial by providing a microenvironment for the differentiation of osteogenic precursor cells to osteoblasts.[10–15] In addition to the porous structure of the β-tricalcium phosphate implants, the biodegradable character of the β-tricalcium phosphate appeared to be advantageous for the regenerative repair of the rib defects, because the progressive replacement of the β-tricalcium phosphate implants by new bone was seen over the time period of this study.[13–15,18,19] The rib defects had been repaired to their original anatomy after removal of the titanium wires from the ribs of animals and resorption of the β-tricalcium phosphate implants at 12 weeks. The use of biomaterials such as hydroxyapatite might repair the rib defects, but bioresorption of implants will not occur. The regenerative repair with restoration of anatomical configuration and degradation of β-tricalcium phosphate implants were most likely achieved through enhanced remodeling of the newly formed bone by the large number of osteoclasts recruited to bone in contact with the β-tricalcium phosphate implant. Bone resorption by osteoclasts is coupled with bone formation by osteoblasts.[20] In this study, osteoblasts, which were differentiated from precursor or stem cells lining the cambium layer of periosteum, may have been involved in the formation and activation of osteoclasts. The close proximity of the osteoclasts to the β-tricalcium phosphate may in turn have enhanced the bone-remodeling rate, leading to the ultimate replacement of the implant material with bone and marrow. In addition, an ability to restore the original anatomy and mechanical strength of the ribs would make this implant methodology unique and potentially useful when used in clin-

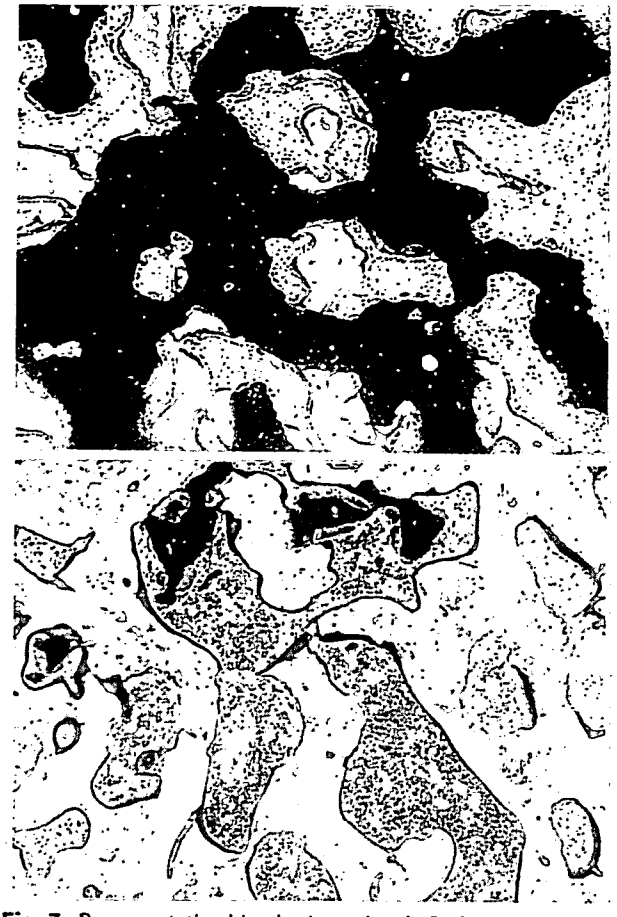

Fig. 7. Representative histologic undecalcified sections in the tricalcium phosphate group (Villaneuva bone stain; original magnification, ×100) at 3 weeks (*above*) and 12 weeks (*below*). At 12 weeks, the β-tricalcium phosphate implant (*black*) was almost completely resorbed, and new bone growth (*pink*) with hematopoietic marrow was seen.

ical practice to regenerate rib defect, only when the periosteum has been left on the chest cage.[10,21]

Limitations of this osteoconductive implant would be the time taken to achieve repair, the reduced mechanical strength of the repaired rib, and the requirement for periosteum. To overcome these problems, the addition of osteoinductive agents such as bone morphogenetic proteins to enhance bone formation both temporally and spatially would be necessary. Attempts to generate these types of implants are ongoing in our laboratory.

CONCLUSIONS

This study demonstrated successful and reproducible regenerative repair of long intercalated rib defects with small cylinders of the biocompatible, osteoconductive biodegradable biomaterial

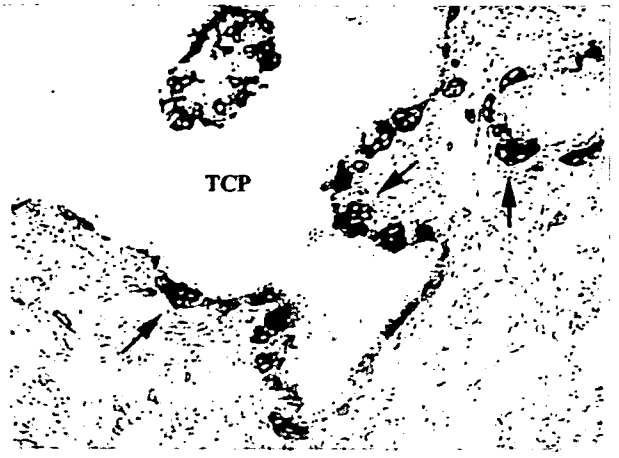

Fig. 8. Representative histologic section at 3 weeks in the tricalcium phosphate group (tartrate-resistant acid phosphatase stain; original magnification, ×200). Multinucleated giant cells were located predominantly on the surface of the porous β-tricalcium phosphate implant (*red, arrows*).

β-tricalcium phosphate, placed in tandem on the periosteum. This type of implant might be useful for the repair of ribs used as a source of bone for reparative or restorative operations.

Masatoshi Hoshino, M.D.
Department of Orthopedic Surgery
Osaka City University Graduate School of Medicine
1-4-3 Asahi-Machi
Abeno-Ku, Osaka 545-8585, Japan
hirotoy@msic.med.osaka-cu.ac.jp

ACKNOWLEDGMENT

This work was supported in part by a Grant-in-Aid from the Ministry of Education, Culture, Sports, Science, and Technology of Japan (Project Grants 16109009 and 16790853).

DISCLOSURE

None of the authors has a financial interest in any of the products, devices, or drugs mentioned in this article.

REFERENCES

1. Nakamura, H., Yamano, Y., Seki, M., et al. Use of folded vascularized rib graft in anterior fusion after treatment of thoracic and upper lumbar lesions: Technical note. *J. Neurosurg. Spine* 94: 323, 2001.
2. Witsenburg, B., Peter, H., and Freihofer, M. Autogenous rib graft for reconstruction of alveolar bone defects in cleft patients: Long-term follow-up results. *J. Craniomaxillofac. Surg.* 18: 55, 1990.
3. Laurie, S. W., Kaban, L. B., Mulliken, J. B., et al. Donor-site morbidity after harvesting rib and iliac bone. *Plast. Reconstr. Surg.* 73: 933, 1984.

4. Whitaker, L. A., Munro, I. R., Salyer, K. E., et al. Combined report of problems and complications in 793 craniofacial operations. *Plast. Reconstr. Surg.* 64: 198, 1979.
5. Mansour, K. A., Thourani, V. H., Losken, A., et al. Chest wall resections and reconstruction: A 25-year experience. *Ann. Thorac. Surg.* 73: 1720, 2002.
6. Deschamps, C., Tirnaksiz, B. M., Darbandi, R., et al. Early and long-term results of prosthetic chest wall reconstruction. *J. Thorac. Cardiovasc. Surg.* 117: 588, 1999.
7. Ayers, R. A., Simski, S. J., Nunes, C. R., et al. Long-term bone ingrowth and residual microhardness of porous block hydroxyapatite implants in humans. *J. Oral Maxillofac. Surg.* 56: 1297, 1998.
8. Akizuki, S., Takizawa, T., and Horiuchi, H. Fixation of a hydroxyapatite-tricalcium phosphate-coated cementless knee prosthesis. *J. Bone Joint Surg. (Br.)* 85: 1123, 2003.
9. Ohura, K., Bohner, M., Hardouin, P., et al. Resorption of, and bone formation from, new beta-tricalcium phosphate-monocalcium phosphate cements: An in vivo study. *J. Biomed. Mater. Res.* 30: 193, 1996.
10. Eggli, P. S., Muller, W., and Schenk, R. K. Porous hydroxyapatite and tricalcium phosphate cylinders with two different pore size ranges implanted in the cancellous bone of rabbits: A comparative histomorphometric and histologic study of bony ingrowth and implant substitution. *Clin. Orthop.* 232: 127, 1988.
11. Ogose, A., Hotta, T., Hatano, H., et al. Histological examination of beta-tricalcium phosphate graft in human femur. *J. Biomed. Mater. Res.* 63: 601, 2002.
12. Ogose, A., Hotta, T., Kawashima, H., et al. Comparison of hydroxyapatite and beta tricalcium phosphate as bone substitutes after excision of bone tumors. *J. Biomed. Mater. Res.* 72: 94, 2005.
13. Dong, J., Uemura, T., Shirasaki, Y., et al. Promotion of bone formation using highly pure porous beta-TCP combined with bone marrow-derived osteoprogenitor cells. *Biomaterials* 23: 4493, 2002.
14. Chazono, M., Tanaka, T., Komaki, H., et al. Bone formation and bioresorption after implantation of injectable beta-tricalcium phosphate granules-hyaluronate complex in rabbit bone defects. *J. Biomed. Mater. Res.* 70A: 542, 2004.
15. Ozawa, M. Experimental study on bone conductivity and absorbability of the pure beta-TCP. *J. Jpn. Soc. Biomater.* 13: 167, 1995.
16. Ishida, H., Tamai, S., Yajima, H., et al. Histologic and biochemical analysis of osteogenic capacity of vascularized periosteum. *Plast. Reconstr. Surg.* 97: 512, 1996.
17. Saito, M., Shimizu, H., Beppu, M., et al. The role of beta-tricalcium phosphate in vascularized periosteum. *J. Orthop. Sci.* 5: 275, 2000.
18. Gosain, A. K., Song, L., Riordan, P., et al. A 1-year study of osteoinduction in hydroxyapatite-derived biomaterials in an adult sheep model: Part I. *Plast. Reconstr. Surg.* 109: 619, 2002.
19. Gosain, A. K., Riordan, P. A., Song, L., et al. A 1-year study of hydroxyapatite-derived biomaterials in an adult sheep model: Part II. Bioengineering implants to optimize bone replacement in reconstruction of cranial defects. *Plast. Reconstr. Surg.* 114: 1155, 2004.
20. Katagiri, T., and Takahashi, N. Regulatory mechanisms of osteoblast and osteoclast differentiation. *Oral Dis.* 8: 147, 2002.
21. Lu, J., Descamps, M., Dejou, J., et al. The biodegradation mechanism of calcium phosphate biomaterials in bone. *J. Biomed. Mater. Res.* 63: 408, 2002.

Comparative roles of Twist-1 and Id1 in transcriptional regulation by BMP signaling

Masanori Hayashi[1,2], Keisuke Nimura[1], Katsunobu Kashiwagi[1], Taku Harada[1], Kunio Takaoka[3], Hiroyuki Kato[2], Katsuto Tamai[1] and Yasufumi Kaneda[1,*]

[1]Division of Gene Therapy Science, Graduate School of Medicine, Osaka University 2-2 Yamada-oka, Suita, Osaka 565-0871, Japan
[2]Department of Orthopedic Surgery, Shinshu University, 3-1-1 Asahi, Matsumoto, Nagano 390-8621, Japan
[3]Department of Orthopedic Surgery, Osaka City University Medical School, 1-4-3 Asahimachi, Abeno-ku, Osaka 545-8585, Japan
*Author for correspondence (e-mail: kaneday@gts.med.osaka-u.ac.jp)

Accepted 12 February 2007
Journal of Cell Science 120, 1350-1357 Published by The Company of Biologists 2007
doi:10.1242/jcs.000067

Summary

Basic helix-loop-helix (bHLH) transcription factors are known as key regulators for mesenchymal differentiation. The present study showed that overexpression of Twist-1, a bHLH transcription factor, suppresses bone morphogenetic protein (BMP)-induced osteoblast differentiation, and downregulation of endogenous Twist-1 enhances BMP signaling. Maximal inhibition of BMP signaling was observed when Twist-1 was bound to E47, which markedly enhanced the stability of Twist-1. Co-immunoprecipitation assays revealed that Twist-1 formed a complex with Smad4 and histone deacetylase (HDAC) 1 in MC3T3-E1 cells stably expressing Twist-1. With trichostatin, an HDAC inhibitor, osteogenic factors such as alkaline phosphatase, Runx2 and osteopontin increased. Those results suggested that Twist-1 inhibited BMP signaling by recruiting HDAC1 to Smad4.

Furthermore, the inhibitory effects of Twist-1 on BMP signaling were overcome by Id1 through induction of Twist-1 degradation. These findings suggest that Twist-1 can act as an inhibitor of BMP signaling, and Id1 can regulate BMP signaling through a positive feedback loop repressing Twist-1 function. These two molecules may therefore regulate differentiation of mesenchymal cells into progeny such as osteoblasts by controlling BMP signaling.

Key words: Twist-1, Id1, BMP, Smad, HDAC

Introduction

Members of the transforming growth factor (TGF)-β superfamily regulate important biological and developmental processes, including cell proliferation, differentiation and migration (Derynck and Zhang, 2003). This is achieved through the ability to induce or repress transcription of diverse gene targets. For example, differentiation of mesenchymal cells into components of bone, cartilage or adipose tissue is regulated by bone morphogenetic proteins (BMPs), which belong to the TGF-β superfamily. BMPs induce not only new bone formation in vivo when implanted into ectopic sites (Urist, 1965), but also osteoblast differentiation of mesenchymal cells in vitro (Katagiri et al., 1994; Thies et al., 1992). TGF-β/BMP signaling is initially mediated by interactions with heterodimeric complexes of type I and type II serine/threonine kinase receptors. Activated receptor kinases phosphorylate receptor-regulated Smads (R-Smads). R-Smads then form activated complexes with common-mediator Smads (C-Smads). These complexes translocate into the nucleus to act as transcriptional regulators (Derynck and Zhang, 2003; Massague, 2000; Wrana, 2000). Studies on the mechanisms by which Smads mediate TGF-β/BMP-regulated gene transcription have led to the discovery of co-activators and co-repressors (Derynck and Zhang, 2003). However, the molecular mechanisms underlying the inhibition of BMP signaling have not been fully elucidated.

Twist-1, originally identified in *Drosophila*, is a member of the basic helix-loop-helix (bHLH) family of proteins (Leptin, 1991; Thisse et al., 1987). Twist-1 is expressed in mesodermal and cranial neural crest cells during embryogenesis (Wolf et al., 1991). In homozygous Twist-1-knockout mice the cranial neural tube fails to close and they die at embryonic day 11.5 (Chen and Behringer, 1995). Twist-1 heterozygous mice present a craniosynostotic phenotype (Bourgeois et al., 1998). Expression of Twist-1 has been implicated in the inhibition of differentiation for multiple mesenchymal cell lineages, including muscle (Hebrok et al., 1997; Spicer et al., 1996) and bone cells (Lee et al., 1999; Rice et al., 2000). The mechanisms of inhibition have been well established in muscle (Hamamori et al., 1999; Hebrok et al., 1997; Spicer et al., 1996), but little is known about the mechanisms behind inhibition of osteoblast differentiation by Twist-1. Very recently, Twist-1 has been reported to interact directly with Runx2, a key transcriptional factor regulating osteogenic gene expression. Direct interaction of Twist-1 with Runx2 causes inhibited DNA binding of Runx2 followed by gene inactivation in osteoblast precursors (Bialek et al., 2004). The fact that neurogenin, another bHLH family member, inhibits glial cell differentiation by sequestering Smad1 of the transcription complex away from glial differentiation genes (Sun et al., 2001), suggests that Twist-1 may likewise affect BMP signaling in the process of mesenchymal cell differentiation into osteoblasts.

The best-studied example of dimerization partners for known tissue-specific bHLH transcription factors involves the gene products of the *E2A* gene (Lassar et al., 1991). Through differential splicing, this gene gives rise to two different bHLH

proteins, E12 and E47, the so-called E-proteins (Murre et al., 1989; Sun and Baltimore, 1991). Id is an internal dominant negative form of HLH transcription factor, lacking a basic region. By sequestering E-proteins, Id prevents myogenic transcription factors, such as MyoD, from forming heterodimer complexes (Benezra et al., 1990; Sun et al., 1991). Recent reports have indicated that BMP induces expression of Id1, resulting in degradation of tissue-specific bHLH transcription factors (Vinals et al., 2004; Vinals and Ventura, 2004). Furthermore, Id1 is critical to BMP-induced osteoblast differentiation (Peng et al., 2004). As a result, we hypothesized that Id1 may be an antagonist of Twist-1 in osteoblast differentiation. The present study found that Twist-1 inhibits BMP-induced osteoblast differentiation. Inhibition of BMP signaling by Twist-1 is enhanced by E-protein. Moreover, the inhibitory effect of Twist-1 is overcome by Id1 through the induction of Twist-1 degradation. These findings suggest that Twist-1 and Id1 can regulate differentiation of mesenchymal cell lineages by controlling BMP signaling.

Results

Overexpression of Twist-1 inhibits BMP-induced osteoblast-specific gene expression

To examine the effect of Twist-1 on expression of BMP2-induced osteoblast differentiation marker genes, a cell line (MC3T3-E1-Tw) stably expressing Twist-1 was established. Since MC3T3-E1 cells contained less endogenous Twist-1 (Tamura and Noda, 1999) and Id1 (data not shown) than C3H10T1/2 cells, the cell line was appropriate to minimize the effect of endogenous Twist-1 and Id1. Exogenous Flag-Twist-1 was detected in MC3T3-E1-Tw1 by western blotting of immunoprecipitates using anti-Flag antibody (Fig. 1A).

Next, ALP activity stimulated by BMP2 was examined. BMP2-induced ALP activity was elevated in parental cells (MC3T3-E1-WT; Fig. 1B). By contrast, Twist-1 overexpression significantly suppressed BMP2-enhanced ALP activity. Basal levels of ALP activity in untreated MC3T3-E1-WT and MC3T3-E1-Tw clone 1 (MC3T3-E1-Tw1) cells were low. We analyzed ALP activity under BMP stimulation in other stable transformant clones. ALP activity in all the clones (data not shown) was much lower than in the parental MC3T3-E1-WT. We further examined whether Twist-1 overexpression also suppressed expression of other osteoblast marker genes, such as osteopontin (Hullinger et al., 2001; Shi et al., 1999; Yang et al., 2000) and osteocalcin (Katagiri et al., 1994; Thies et al., 1992). The level of BMP2-induced osteopontin expression in MC3T3-E1-Tw1 cells was lower than in MC3T3-E1-WT cells. BMP2-induced osteocalcin expression also decreased in MC3T3-E1-Tw1 cells (Fig. 1C). These results indicate that Twist-1 could affect BMP2-induced osteoblast differentiation.

Downregulation of endogenous Twist-1 enhances transcriptional activity mediated by BMP signaling

To examine the function of Twist-1 in BMP signaling, we attempted to downregulate endogenous Twist-1 expression in C3H10T1/2, a mesenchymal progenitor cell line with high levels of Twist-1 expression, using RNA interference (RNAi) technology. We selected the most effective Twist-1-specific siRNA (siTwist-691). Transient transfection of siTwist-691 resulted in a 50-60% decreases in mRNA levels (Fig. 2A). Next, we examined the direct effects of downregulating

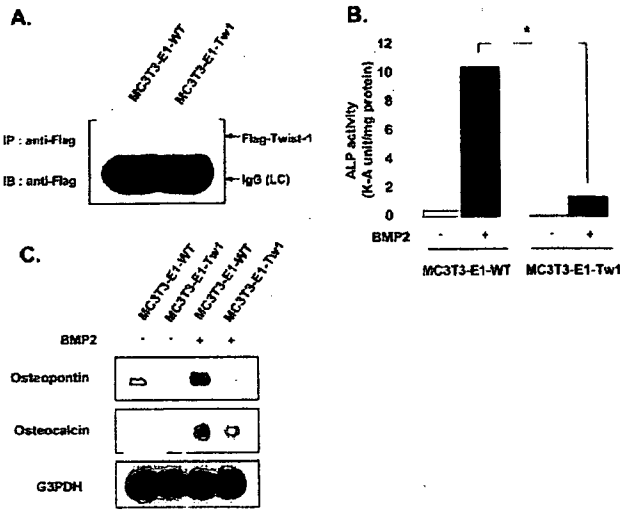

Fig. 1. Twist-1 overexpression suppresses BMP2-induced osteoblast differentiation. (A) Immunoprecipitation of overexpressed Flag-tagged Twist-1 in the nuclear extracts of MC3T3-E1-Tw1 and MC3T3-E1-WT cells. (B) MC3T3-E1-Tw1 and MC3T3-E1-WT cells were grown in the presence or absence of rhBMP2 (300 ng/ml) for 6 days. ALP activity was measured as described in the Materials and Methods (*P<0.01). (C) MC3T3-E1-Tw1 and MC3T3-E1-WT cells were grown in the presence or absence of rhBMP-2 (300 ng/ml) and total RNA was isolated on day 6. Northern blot analysis was performed using osteopontin and osteocalcin cDNA probes.

endogenous Twist-1 on transcriptional activity mediated by Smads using 3GC2-Lux, which contains three tandem repeats of a Smad-binding GC-rich sequence linked with the collagen X core promoter inserted into pGL2-Basic (Ishida et al., 2000). 24 hours after transfection of C3H10T1/2 cells with Twist-1-specific siRNA, cells were transfected with 3GC2-Lux and TK-*Renilla* luciferase and fed with or without rhBMP2 treatment. Suppression of endogenous Twist-1 expression by Twist-1-specific siRNA resulted in increased BMP-dependent Smad transcriptional activity (Fig. 2B). Additionally, when the siTwist-691 was co-transferred to C3H10T1/2 cells with Twist-1 expression plasmid by lipofection, real-time PCR analysis indicated that endogenous Twist-1 expression was partially recovered (at most 32% compared with Twist-1 level in the cells received the siRNA alone). However, no significant increase of endogenous Twist-1 expression was obtained using control plasmid, pCAGIP, without Twist-1 cDNA (data not shown).

Next, we overexpressed Smad1, Smad4 and BMPR-IB(QD) in C3H10T1/2. Downregulation of endogenous Twist-1 using Twist-1-specific siRNA also enhanced transcriptional activity mediated by overexpressed Smads (Fig. 2C). These results indicate that Twist-1 could inhibit BMP/Smad signaling.

Twist-1 inhibits BMP signaling cooperatively with E-protein

To examine whether overexpressed Twist-1 could inhibit BMP-induced transcriptional activity, co-transfection studies were performed. P19 cells that respond to BMPs and express some of the BMP target genes were transfected using Twist-1,

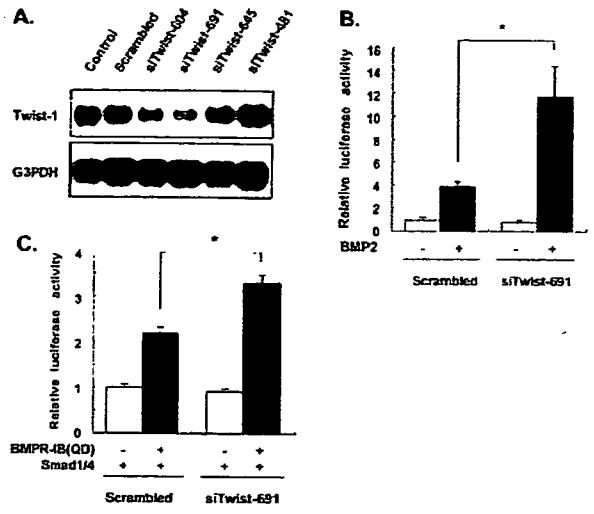

Fig. 2. Downregulation of endogenous Twist-1 using RNAi methods enhances BMP-induced transcriptional activity mediated by Smads. (A) C3H10T1/2 cells were transfected with either Twist-1-specific siRNA (siTwist-604, siTwist-691, siTwist-645, siTwist-481) or control siRNA (Scrambled) as described in the Materials and Methods. Total RNA was extracted 24 hours later, and northern blot analysis was performed using a Twist-1 cDNA probe. (B) C3H10T1/2 cells were transfected with either siTwist-691 or control siRNA (Scrambled). Cells were transfected with 3GC2-Lux and TK-*Renilla* luciferase 24 hours after siRNA transfection. At 12 hours after second transfection, cells were treated, with BMP (300 ng/ml) or left untreated, for 12 hours. Cells were lysed and luciferase activity was assayed (*P<0.01). The mean value of firefly luciferase and *Renilla* luciferase activity in the scrambled sample without BMP was approximately 2,000 and 34,000 RLU (relative light unit), respectively. (C) C3H10T1/2 cells were transiently transfected with either 90 pmol of siTwist-691 or Scrambled in combination with 100 ng of 3GC2-Lux luciferase construct, Smad1, Smad4 and BMPR-IB(QD). Cells were lysed and luciferase activity was assayed 24 hours after transfection (*P<0.01). The mean value of firefly luciferase and *Renilla* luciferase activity in the scrambled sample without BMPR-1B(QD) was approximately 411,000 and 30,000 RLU, respectively.

Smad1 and Smad4 expression constructs and 3GC2-Lux containing a Smad-binding sequence. Co-transfection of BMPR-IB(QD) with Smad1 and Smad4 enhanced transcription of 3GC2-Lux (Fig. 3A). Exogenous Twist-1 inhibited this activity, but inhibitory effects were very weak. Since Twist-1 reportedly inhibits MyoD trans-activation by E-protein sequestration, and the Twist-1-E-protein heterodimer inhibits myocyte enhancer-binding factor 2 (MEF2) trans-activation by direct interaction (Spicer et al., 1996), we hypothesized that the Twist-1-E-protein heterodimer could also act as a repressor in BMP signaling. We examined the effects of E47, an alternatively spliced product of the *E2A* gene (Murre et al., 1989; Sun and Baltimore, 1991), on suppression of Smad signaling by Twist-1. Twist-1 bound to E47 further increased the inhibition of BMP-induced transcription of 3GC2-Lux in a dose-dependent manner (Fig. 3A).

Next, the effect of Twist-1 and E47 on TGF-β signaling was analyzed using 3TP-Lux, which was empirically designed to have maximal responsiveness to TGF-β (Wrana et al., 1992). However, TGF-β signaling was not inhibited by Twist-1 and E47. Id proteins are dominant-negative-type HLH proteins that lack the basic DNA-binding domain. In muscle development, Id1 forms heterodimers with E-protein and prevents myogenic bHLH proteins from forming complexes with E-protein (Benezra et al., 1990; Sun et al., 1991). BMP stimulation also reportedly induces Id1 expression (Katagiri et al., 1994; Nakashima et al., 2001; Ogata et al., 1993), an adverse pattern as compared to Twist-1 expression (Tamura and Noda, 1999). We therefore investigated whether Id1 also cooperated with E-protein to inhibit BMP signaling. In contrast to Twist-1, however, Id1 failed to repress BMP signaling in the presence or absence of E47 (Fig. 3B), suggesting distinctly different roles for Id1 and E47 in BMP signaling. Moreover E47 also failed to repress Smad signaling without Twist-1 (Fig. 3B). To assess whether formation of heterodimer complex with E-protein is critical for the inhibitory effect of Twist-1, we overexpressed a Twist-1 mutant (Twist-NBCT), which lacks the HLH domain (El Ghouzzi et al., 2000; Hamamori et al., 1997; Hebrok et al., 1997; Spicer et al., 1996). This Twist-1 mutant did not interact with E-protein (Fig. 3C). In contrast to with wild-type Twist-1, Twist-NBCT failed to suppress transcriptional activity in the presence or absence of E47 (Fig. 3D). These findings suggest that maximal inhibition of BMP signaling by Twist-1 requires heterodimer formation with E-protein. Additionally, by over expression of Twist-1 and E47, the inhibition of luciferase gene expression by siRNA was abolished (Fig. 3E).

Twist-1 inhibited BMP signaling by recruiting HDAC1 to the Smad1-Smad4 complex

Histone deacetylases (HDACs) are involved in the repression of MyoD and MEF2 by Twist-2, which shares high homology with Twist-1 (Gong and Li, 2002; Li et al., 1995; Tamura and Noda, 1999). To analyze the involvement of HDAC in the inhibition of BMP signaling by Twist-1, Flag-tagged Twist-1 was immunoprecipitated using anti-Flag antibody in MC3T3-E1-Tw1 and the presence of HDAC and Smad was investigated in the precipitate. As shown in Fig. 4A, HDAC1 and Smad4 were detected in the precipitate, but not Smad1. In MC3T3-E1-WT, neither HDAC1 nor Smad4 was precipitated. Next, trichostatin (TSA), an HDAC inhibitor, was used to rescue the inhibition of osteogenic gene expression mediated by Twist-1. As shown in Fig. 4B, TSA treatment significantly increased the expression of ALP, Runx2 and osteopontin in the MC3T3-E1-Tw1 under BMP2 stimulation. These results suggested that Twist-1could inhibit BMP signaling by recruiting HDAC1 to Smad complex via Smad4.

Twist-1 protein stability is increased by the formation of heterodimer complex with E-protein

Stability of bHLH proteins is reportedly increased by the formation of heterodimer complexes with other bHLH proteins (Deed et al., 1996; Vinals et al., 2004; Vinals and Ventura, 2004). We therefore examined whether co-expression of E47 increases the level of Twist-1 protein. Myc-tagged Twist-1 was expressed with or without Myc-tagged E47 in COS-7 cells, and the levels of both were immunodetected by western blotting. Co-expression of E47 greatly increased Twist-1 protein levels (Fig. 5A). Next, to determine whether enhancement of Twist-1 protein expression is caused by

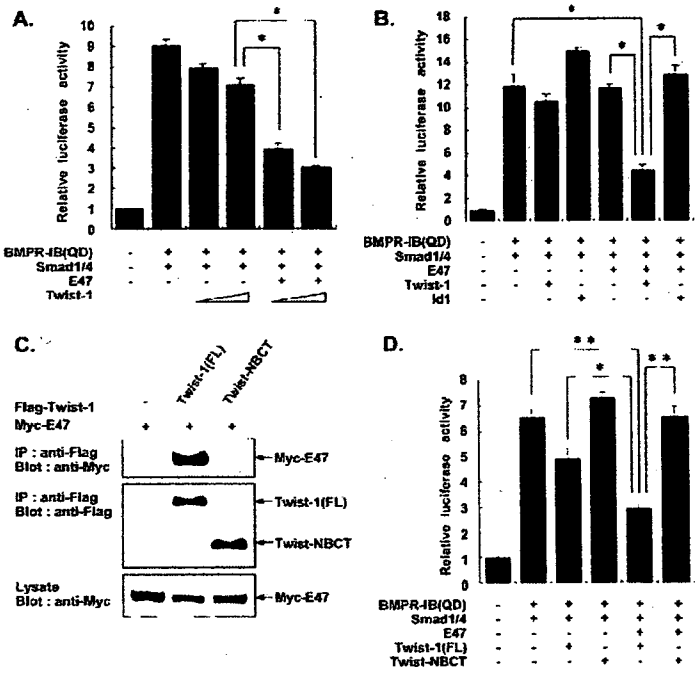

Fig. 3. Twist-1 inhibits BMP-induced Smad transcriptional activity with E-protein. (A) P19 cells were transiently transfected with 3GC2-Lux luciferase construct in combination with 50 ng of BMPR-IB(QD), Smad1, Smad4, E47 and increasing doses (12.5 or 50 ng) of Twist-1 expression construct. Cells were lysed and luciferase activity was assayed 24 hours after transfection (*P<0.01). The mean value of firefly luciferase and *Renilla* luciferase activity in cells transfected with luciferase expression plasmids was approximately 109,000 and 681,000 RLU, respectively. (B) P19 cells were transiently transfected with 3GC2-Lux luciferase construct in combination with 50 ng of BMPR-IB(QD), Smad1, Smad4, E47, Twist-1 and Id1 construct. Cells were lysed and luciferase activity was assayed 24 hours after transfection (*P<0.01). The mean value of firefly luciferase and *Renilla* luciferase activity in cells transfected with luciferase expression plasmids was approximately 51,000 and 199,000 RLU, respectively. (C) Flag-tagged full-length (FL) Twist-1 or deletion Twist-1 mutant (Twist-NBCT) and Myc-tagged E47 constructs were transfected into COS-7 cells. Lysates were immunoprecipitated using anti-Flag antibody and blotted with anti-Myc antibody. (D) P19 cells were transiently transfected with 3GC2-Lux luciferase construct in combination with 50 ng of BMPR-IB(QD), Smad1 and Smad4, E47, full-length Twist-1 and deletion Twist-1 mutant (Twist-NBCT) expression construct. Cells were lysed and luciferase activity was assayed 24 hours after transfection (**P<0.01, *P<0.05).

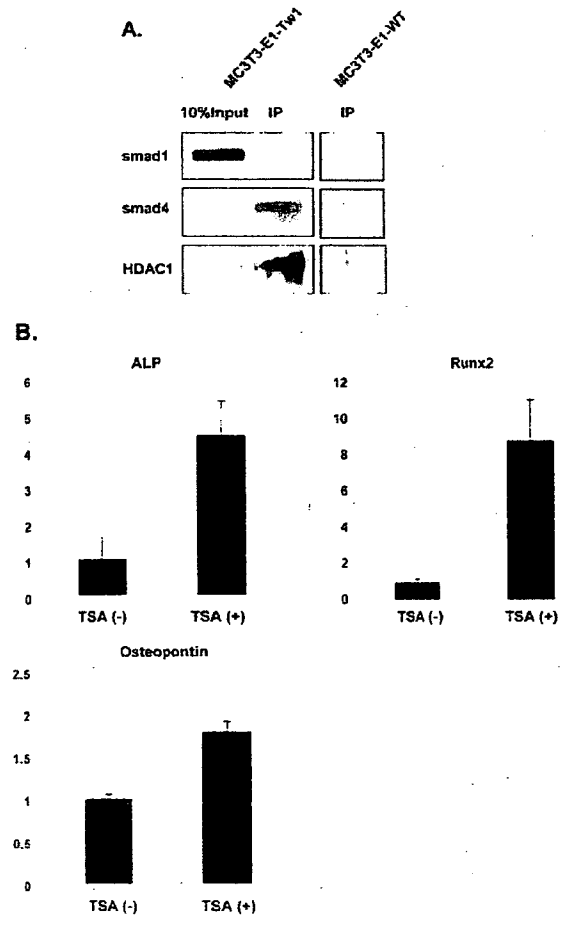

avoidance of degradation, we examined Twist-1 protein turnover using a pulse-chase assay. Twist-1 was rapidly degraded in cells, with protein levels at 180 minutes reduced to 17% compared with the baseline at 0 minutes. By contrast, Twist-1 protein stability was greatly enhanced by co-expression with E47 (Fig. 5B). Recent reports have shown that Id genes are rapidly upregulated by BMP stimulation (Nakashima et al., 2001; Ogata et al., 1993; Peng et al., 2004). BMP2 decreases myogenin and Mash1 protein stability through induction of Id1 (Vinals et al., 2004; Vinals and Ventura, 2004). In addition, our previous data showed that Twist-1 could inhibit BMP signaling (Fig. 3A,B,D). These results prompted us to investigate whether Id1 would induce Twist-1 degradation and inhibit Twist-1 function. Twist-1 was degraded by co-transfection of Id1 in the presence of E47 (Fig. 5B).

Id1 inhibits Twist-1 function by interfering with functional Twist-1-E47 heterodimer formation

The finding that Twist-1 stabilization by E47 was partially lost by co-transfection of Id1 suggests that Id1 may sequester E47 from Twist-1, resulting in Twist-1 degradation. We tested this

Fig. 4. Twist-1 can interact with HDAC1 and Smad4. (A) MC3T3-E1-WT and MC3T3-E1-Tw1 cells were treated with BMP2 (300 ng/ml) for 24 hours. Lysates were immunoprecipitated using anti-Flag antibody and blotted with anti-Smad4 and HDAC1 antibody. 10% In, 10% of input; IP, immunoprecipitated fraction. (B) MC3T3-E1-Tw1 cells were treated with BMP alone [TSA (–)] or the mixture of BMP and TSA (82.5 μM) [TSA (+)]. After 24 hours, total RNA was extracted and the expression of ALP, Runx2 and osteopontin was quantified by real-time PCR. The expression levels were normalized by GAPDH, and the ratio was shown in each sample. Data are presented as mean ± s.d. of triplicate samples (*P<0.05).

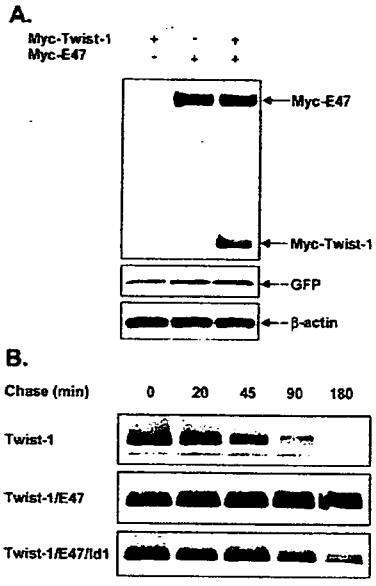

Fig. 5. Twist-1 protein stability is increased by the formation of a heterodimer complex with E47. (A) Myc-tagged Twist-1 and E47 constructs and GFP expression vector were transfected into COS-7 cells. Western blot analysis was performed with anti-Myc antibody. To show transfection efficiency, GFP protein was also detected by western blot. (B) COS-7 cells were transfected with the Flag-tagged Twist-1, Myc-tagged E47 and/or Myc-tagged Id1. At 24 hours after transfection, cells were pulsed with [^{35}S]methionine and cysteine for 3 hours, and chased with unlabeled medium for the indicated times. Labeled cell lysates were immunoprecipitated using anti-Flag antibody. Flag-tagged Twist-1 was visualized using SDS-PAGE.

possibility using immunoprecipitation assay in COS-7 cells. Increasing doses of Id1 decreased the amounts of E47 co-immunoprecipitated with Twist-1 (Fig. 6A). The amount of immunoprecipitated Twist-1 was also decreased by co-transfection of Id1, suggesting that Id1 induces Twist-1 degradation by sequestering E47 from Twist-1.

To examine whether Twist-1 also interferes with Id1-E47 heterodimer formation, we next performed the same experiment by replacing Id1 with Twist-1. In contrast to Id1, Twist-1 failed to interfere with Id1-E47 heterodimer formation (Fig. 6B). These results suggest that Id1 interacts with E47 more strongly than Twist-1 does, resulting in sequestration of E47 from Twist-1. In C3H10T1/2, endogenous Id1 was also co-immunoprecipitated with E47 using anti-E47 antibody (Fig. 6C). We examined the possibility that Id1 could rescue the inhibitory effect of Twist-1 on BMP signaling by inducing Twist-1 degradation. Twist-1-induced inhibition of BMP signaling was overcome by Id1 in a dose-dependent manner (Fig. 6D). It has been reported that differentiation of osteoblastic cells is promoted by transient expression of Id1 in early developmental stages (Peng et al., 2004). We attempted to rescue the inhibition of BMP signaling by Id1 gene transfer to MC3T3-E1-Tw1. As shown in Fig. 6E, the recovery of ALP activity in MC3T3-E1-Tw1 by Id1 gene transfer was significantly higher than by GFP gene transfer. These findings indicate that Id1 may regulate BMP signaling through a positive feedback loop that represses Twist-1 function.

Discussion

During embryonic mesoderm development, BMPs play critical roles in the commitment of mesenchymal cells into osteoblast and chondroblast lineages (Centrella et al., 1994; Hogan, 1996). Smads phosphorylated by BMP stimulation translocate into the nucleus and interact in transcription complexes with several DNA-binding transcription factors or cofactors that affect gene activation (Derynck and Zhang, 2003; Massague, 2000; Wrana, 2000). These factors have been considered critical for a variety of responses to BMP signaling in different BMP-targeted genes. Also, several inhibitors of BMP signaling have been reported. For example, Smad6 inhibits BMP/Smad1 signaling by acting as a selective Smad4 decoy (Hata et al., 1998). Tob, a member of the anti-proliferative protein family, binds Smad1, Smad5 and Smad8, and inhibits Smad-mediated transcriptional activities (Yoshida et al., 2000). Smads have also been shown to interact with bHLH transcription factors. For example, Smad3 directly interacts with MyoD and represses transcriptional activity (Liu et al., 2001). Neurogenin, another bHLH transcription factor, binds to both Smad1 and CBP (CREB-binding protein), and inhibits glial differentiation (Sun et al., 2001). The present study provides the first report that Twist-1, a DNA-binding bHLH transcription factor, inhibits transcriptional activities mediated by Smads (Fig. 3A,B,D).

Twist-1 reportedly acts as an inhibitor of muscle differentiation by sequestering E-protein from MyoD and blocking DNA binding, and by inhibiting trans-activation by MEF2 (Spicer et al., 1996). Twist-2 also requires heterodimerization with E-protein for inhibition of MyoD and MEF2 (Gong and Li, 2002), as seen with Twist-1. In addition, HDACs are involved in the repression of MyoD by Twist-1 and -2. In our results, Twist-1 also required heterodimerization with E47 for both maximal inhibition of Smad-mediated transcriptional activity (Fig. 3A,B,D) and increasing Twist-1 protein stability (Fig. 5B). BMPs activate transcription through physical interaction and functional cooperation of R-Smads and coactivators CBP and/or p300 (Derynck and Zhang, 2003). Our result (Fig. 4A,B) supports the possibility that the inhibition of BMP signaling by Twist-1 and E47 was mediated by direct recruitment of HDAC1 to Smad complexes via Smad4. The repression of HDAC by TSA increased the expression of osteogenic factors probably by the activation of BMP signaling. However, gel-shift assay of Smads revealed that Twist-1 failed in the inhibition of DNA binding of Smads (data not shown). This result was not contradictory to the involvement of HDAC in inhibitory mechanism by Twist-1.

We also showed that the effect of Twist-1 in repressing BMP signaling was abrogated by Id1 (Fig. 6D,E). Id1 expression is induced by BMP stimulation in mesenchymal and neuroepithelial cells (Katagiri et al., 1994; Nakashima et al., 2001; Ogata et al., 1993). Id1 lacks the basic region necessary for binding to the E-box and acts as a dominant negative regulator by sequestering E-protein (Benezra et al., 1990). Furthermore, Id1 sequesters E-proteins away from myogenin and inhibits myogenesis by accelerating myogenin degradation (Vinals and Ventura, 2004). In neural development, transient induction of Id1 by BMP2 decreases Mash1 stability and restricts neuronal differentiation by the same mechanism (Vinals et al., 2004). These findings support the possibility that Id1 may positively regulate BMP signaling

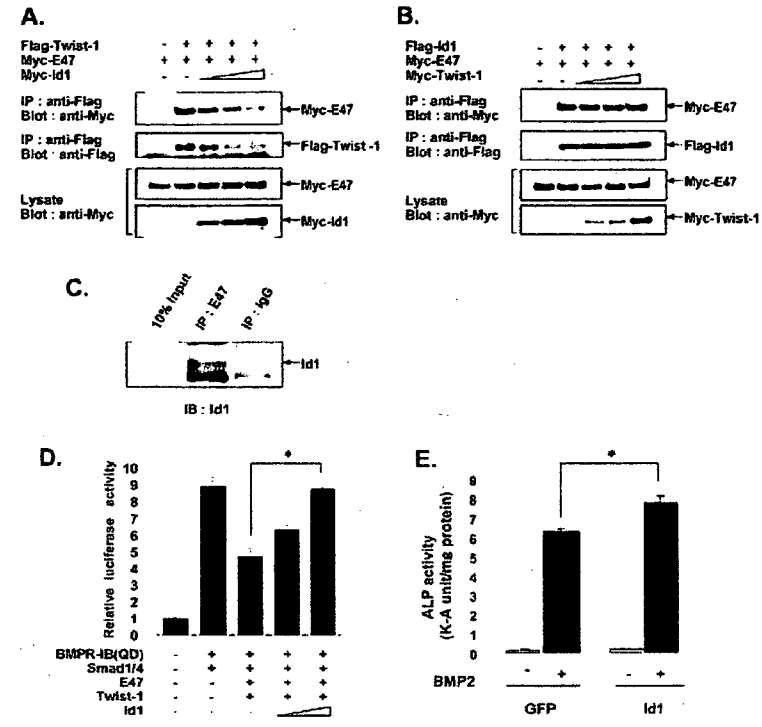

Fig. 6. Id1 inhibits Twist-1 function by sequestering E47 from Twist-1. (A) COS-7 cells were transiently transfected with Flag-Twist-1, Myc-tagged E47 and increasing doses (0.5, 1 or 2 μg) of Myc-tagged Id1 construct. Lysates were immunoprecipitated using anti-Flag antibody and blotted with anti-Flag and anti-Myc-antibody. (B) COS-7 cells were transiently transfected with Flag-Id1, Myc-tagged E47 and increasing doses (0.5, 1 or 2 μg) of Myc-tagged Twist-1 construct. Lysates were immunoprecipitated using anti-Flag antibody and blotted with anti-Flag and anti-Myc-antibody. (C) Endogenous E47 in C3H10T1/2 cells was precipitated using anti-E47 antibody. Then, Id1 was detected in the immunoprecipitates by western blot. (D) P19 cells were transiently transfected with 3GC2-Lux luciferase construct in combination with 50 ng of BMPR-IB(QD), Smad1 and Smad4, 25 ng of Twist-1 and E47, and increasing doses (25 or 100 ng) of Id1 expression construct. Cells were lysed and luciferase activity was assayed 24 hours after transfection (*P<0.01). (E) MC3T3-E1-Tw1 cells were transiently transfected with either Id1 or GFP expression construct by electroporation (Amaxa). The cells were grown in the presence or absence of rhBMP2 (300 ng/ml) for 6 days. ALP activity was measured as described in the Materials and Methods. Data are presented as mean ± s.d. of triplicate samples (*P<0.05).

by sequestering E-protein from Twist-1 to accelerate degradation. As shown in Fig. 6E, the recovery of ALP activity in MC3T3-E1-Tw1 by Id1 gene transfer was significantly higher than by GFP gene transfer, but the effect was not as much as expected from co-transfection experiment (Fig. 6D). We estimated that transient expression of Id1 was not sufficient to completely overcome the effect of stably expressing Twist-1, because transfection efficiency was not as high (at most 20%) in MC3T3-E1 cells.

In response to BMP stimulation, C3H10T1/2 embryonic mesenchymal cells express bone markers including collagen type I, ALP, osteopontin and osteocalcin (Ju et al., 2000). The osteopontin gene is reportedly a target of the BMP signaling pathway. Smad1 activates the osteopontin promoter by preventing Hoxc-8 (which negatively regulates osteopontin expression) from binding to this promoter (Shi et al., 1999; Yang et al., 2000). In addition, BMP stimulates direct binding of Smad proteins to the targeting sequence of the osteopontin promoter and activates transcription (Hullinger et al., 2001). In this study, we found that overexpression of Twist-1 repressed BMP2-induced expression of osteopontin and osteocalcin, and ALP activity (Fig. 1B,C). It is also known that Runx2 activates the expression of ALP, osteopontin and osteocalcin (Ducy et al., 1997; Harada et al., 1999). Furthermore, Twist-1 directly inhibits Runx2 (Bialek et al., 2004). From these reports, there is a possibility that the inhibition of BMP signaling in our experiments might result from an indirect effect mediated by the inhibition of Runx2. However, by direct binding with Runx2, Smads activate the transcription of Runx2 (Lee et al., 2000; Zhang et al., 2000). Moreover, BMP signaling was suppressed in co-transfection experiments using a reporter gene without the Runx2 recognition DNA sequence, as shown in Fig. 3A,B. Therefore, in addition to an indirect effect, through the inhibition of Runx2, it is likely that Twist-1 may have a direct inhibitory effect on BMP signaling.

We also showed that Smad-dependent transcriptional activity was enhanced by siRNA-mediated downregulation of endogenous Twist-1 in transient transfection analysis with a reporter construct containing BMP-responsive elements (Fig. 2B,C). Levels of Twist-1 expression gradually decrease during osteoblast differentiation (Bialek et al., 2004; Rice et al., 2000; Tamura and Noda, 1999). Taken together these results indicate that Twist-1 may maintain the population of undifferentiated mesenchymal cells by inhibiting BMP-induced osteoblast differentiation. Our data indicate a novel mechanism by which the cellular effects of BMP signals can be potentially regulated through direct competition between Twist-1 and Id1 for binding to E-protein.

Materials and Methods

Plasmid construction

Mouse Twist-1, E47, Id1 and Smad1 and Smad4 were amplified using polymerase chain reaction (PCR) from cDNA templates, which were reverse transcribed from mRNA of C3H10T1/2. To create mammalian expression vectors Myc-Twist-1, E47, Id1, Flag-Twist-1, Smad1 and Smad4, cDNA clones were introduced using Gateway technology (Invitrogen, San Diego, CA) into pCAGIP-Myc and pCAGIP-Flag vectors (Niwa et al., 2002). For Flag-Twist-1 deletion mutants, Twist-NBCT (deletion of amino acids 125-169) were created by PCR, then introduced into pCAGIP-Flag using Gateway technology. To generate mammalian expression vectors pCMV-Twist-1, pCMV-E47, pCMV-Id1 and pCMV-Smad1 and pCMV-Smad4, the corresponding cDNA clones were introduced with Gateway technology into pcDNA3.1 (Invitrogen), which was converted into the destination vector. A 3GC2-Lux luciferase construct, the constitutively active form of BMP type I receptor [BMPR-IB(QD)] (Imamura et al., 1997) and the constitutively active form of TGF-β type I receptor [TβR-I(TD)] (Wieser et al., 1995) were kindly donated by Kohei Miyazono (University of Tokyo).

Cell culture and stable transfection

The C3H10T1/2 murine mesenchymal progenitor cell line, MC3T3E-1 osteoblastic cell line and COS-7 African green monkey SV40-transformed kidney fibroblast

cells line were cultured in Dulbecco's modified Eagle's medium (DMEM) supplemented with 10% heat-inactivated fetal bovine serum (FBS) and antibiotics. The P19 murine teratocarcinoma cell line was cultured in α-modified Eagle's medium supplemented with 10% FBS and antibiotics. Twist-1-overexpressing MC3T3-E1 (MC3T3-E1-Tw1) cells were obtained by puromycin selection of MC3T3-E1 cells transfected with pCAGIP-Flag-Twist-1. Screening of Twist-1-overexpressing clones was performed by western blotting of immunoprecipitates using anti-Flag antibody.

siRNA method

Target short interfering RNA (siRNA) was determined using the siRNA design tool (Invitrogen). The siTwist-604 sense sequence was 5′-AAGCUGAGCAAGAUUCAGACC-3′; siTwist-691 sense sequence was 5′-AAGAUGGCAAGCUGCAGCUAU-3′; siTwist-645 sense sequence was 5′-CAUCGACUUCCUGUACCAGGU-3′; and siTwist-481 sense sequence was 5′-CAGUCGUACGAGGAGCUGCAG-3′. As a control, the non-silencing siRNA sense sequence was 5′-AAGCGCGCUUUGUAGGAUUCG-3′. C3H10T1/2 cells were seeded at 70% confluence on the day before transfection. Transfections were performed using Lipofectamine 2000 transfection reagent (Invitrogen). To examine the effects of Twist-1-specific siRNA on reporter constructs, cells were transfected with 3GC2-Lux and pRL-TK vector (Promega, Madison, WI) using FuGENE6 transfection reagent (Roche, Basel, Switzerland) 24 hours after siRNA transfection. At 36 hours after siRNA transfection, cells were treated with rhBMP2 (300 ng/ml) for 12 hours. Both firefly and *Renilla* luciferase activities were measured 2 days after siRNA transfection using a dual luciferase assay system (Promega). Co-transfections of siRNA and plasmid DNAs were performed using X-treamGENE siRNA transfection reagent (Roche).

RNA extraction and northern blot analysis

Total RNA was isolated using Isogen (Nippon Gene, Tokyo, Japan) according to the instructions of the manufacturer. Total RNA (15 μg) was denatured, electrophoresed in 2% agarose gels containing 18% formaldehyde, then transferred to Hybond-N+ membrane (Amersham Biosciences, Piscataway, NJ). Membranes were hybridized at 65°C for 12 hours in a hybridization buffer, PerfectHyb (Toyobo, Osaka Japan). Probes for Twist-1, osteocalcin, osteopontin and G3PDH were labeled using the RadPrime DNA labeling system (Invitrogen). After hybridization, membranes were washed four times with 2× standard sodium citrate (SSC) and 0.1% sodium dodecyl sulfate (SDS). Blots were exposed to X-ray films using intensify screens at –80°C.

Alkaline phosphatase assay

Alkaline phosphatase (ALP) activity was assessed as previously described (Wakabayashi et al., 2002). Briefly, cell lysates were centrifuged and supernatants were used for enzyme assays. ALP activity was measured according to the methods of Kind-King, using a test kit (Wako, Osaka, Japan) with phenylphosphate as a substrate. Enzyme activity was expressed in King-Armstrong (K-A) units, normalized to protein concentration. Results are presented as mean ± standard deviation (s.d.) from a representative experiment. Statistical analysis was performed using analysis of variance (ANOVA).

Transfections and reporter assays

P19 cells were transiently transfected using 3GC2-Lux together with expression constructs of Smad1, Smad4, Twist-1, E47, Id1 and BMPR-IB(QD) using FuGENE6 transfection reagent. P19 cells were chosen because the cells responded to BMPs and expressed some of the BMP target genes. Additionally, transfection efficiency was higher in P19 cells than in other cell lines. At 24 hours after transfection, both firefly and *Renilla* luciferase activities were assayed with the dual luciferase assay system (Promega) using a Lumat LB 9507 luminometer (Berthold Technologies, Wildbad, Germany). Firefly luciferase activity was normalized with respect to *Renilla* luciferase activity. All assays were performed at least three times in duplicate or triplicate. Results are presented as mean ± s.d. from a representative experiment. Statistical analysis was performed using ANOVA.

Immunoprecipitation and immunoblotting

COS-7 cells were transiently transfected with the expression construct using FuGENE6 transfection reagent. COS-7 cells were used because they contained no endogenous Twist-1. At 24 hours after transfection, cells were lysed in buffer containing 25 mM Hepes pH 8.0, 150 mM KCl, 2 mM EDTA, 0.1% Nonidet P-40 (NP-40) and EDTA-free complete protease inhibitor cocktail (Roche). After 20 minutes on ice, cell lysates were pelleted by centrifugation and supernatants were pre-cleared with normal mouse IgG (Santa Cruz, Santa Cruz, CA) for 30 minutes at 4°C, then incubated with anti-FLAG M2 affinity gel (Sigma, St Louis, MO) for 4 hours at 4°C. Immunoprecipitates were washed four times with the buffer used for cell solubilization. Immune complexes were eluted at 98°C for 5 minutes in Laemmli's sample buffer. Immunoprecipitates were separated by SDS-polyacrylamide gel electrophoresis (PAGE), transferred to polyvilinidendifluoride (PVDF) membrane, and immunoblotted with anti-Flag M2 antibody (Sigma) and anti-Myc antibody (MBL, Nagoya Japan). Protein bands were visualized using Chemi-Lumi One (Nacalai Tesque, Kyoto, Japan).

To detect overexpressed Smad1 and Smad4, P19 cells were lysed as described above, 24 hours after transfection. Lysates were separated by SDS-PAGE, transferred to PVDF membrane, and immunoblotted with anti-Smad1 and -Smad4 antibody (Santa Cruz) and anti-β-actin antibody (ABcam, Cambrige, UK). Protein bands were visualized using Chemi-Lumi One (Nacalai Tesque).

Nuclear protein extracts were prepared from MC3T3-E1 cells as follows. Cells were harvested by centrifugation at 500 *g* for 10 minutes at 4°C. Cell pellets were washed by gentle resuspension in cold PBS-0.5 mM EDTA and nuclei isolation buffer (NIB) containing 10 mM Tris-HCl (pH 7.5), 60 mM KCl, 15 mM NaCl, 1.5 mM $MgCl_2$, 1 mM $CaCl_2$, 0.25 M sucrose, 10% glycerol, 0.1 mM phenylmethylsulfonylfluoride (PMSF) and EDTA-free complete protease inhibitor cocktail (Roche). Cells were re-suspended with ice-cold NIB containing 0.1% NP-40 and allowed to swell for 10 minutes on ice. Swollen cells were centrifuged at 500 *g* for 10 minutes at 4°C. Nuclei pellets were washed in cold NIB and centrifuged at 500 *g* for 5 minutes at 4°C. Nuclear pellets were diluted to 1.5 mg/ml DNA with ice-cold NIB and digested using micrococcal nuclease (80 units/mg DNA; Worthington, Lakewood, NJ). Digested nuclei were rapidly cooled on ice for 10 minutes and centrifuge at 12,800 *g* for 10 minutes at 4°C. Supernatant (S1) was collected and pellets were re-suspended with ice-cold cell lysis buffer containing 10 mM Tris-HCl (pH 7.5), 2 mM EDTA, 10% glycerol, 300 mM NaCl, 0.1 mM PMSF and EDTA-free complete protease inhibitor cocktail (Roche), then incubated for 45 minutes on ice. Nuclear debris was spun out by centrifugation at 12,800 *g* for 10 minutes at 4°C, and the supernatant (S2) was collected. S1 and S2 fractions were combined, then incubated with anti-Flag M2 affinity gel (Sigma) for 4 hours at 4°C. Immunoprecipitates were washed four times with cell lysis buffer containing 0.1% NP-40. Immune complexes were eluted at 98°C for 5 minutes in Laemmli's sample buffer. Immunoprecipitates were separated by SDS-PAGE, transferred to PVDF membrane, and immunoblotted using anti-Flag M2 antibody (Sigma).

To analyze the interaction of Id1 and E47, or Smad4, HDAC1 and Flag-Twist-1, C3H10T1/2 and MC3T3-E1-Tw1 cells were lysed with RIPA buffer containing 50 mM Tris-HCl (pH 7.4), 1% NP-40, 0.25% sodium deoxycholate, 150 mM NaCl, 1 mM EDTA and EDTA-free complete protease inhibitor cocktail (Roche), and the supernatant was obtained by centrifugation of the lysates at 12,800 *g* for 5 minutes at 4°C. After the removal of non-specifically bound substances using non-immune IgG (Santa Cruz), the supernatant was incubated with anti-E47 (Santa Cruz) antibody for 2 hours at 4°C and precipitated with protein A beads, or anti-Flag M2 affinity gel for 4 hours at 4°C. After washing the precipitates four times with the RIPA buffer, immune complexes were eluted at 98°C for 5 minutes in Laemmli's sample buffer. Immunoprecipitates were separated by SDS-PAGE, transferred to PVDF membrane, and immunoblotted using anti-Id1, anti-Smad4 (Santa Cruz), anti-Smad1 (Zymed, San Francisco, CA), anti-HDAC1(Upstate Temecula, CA) antibodies.

Pulse-chase assay

Pulse-chase assay was performed according to the method previously described (Deed et al., 1996), with minor modification. COS-7 cells were transfected with Flag-Twist-1, Myc-E47 and Myc-Id1 using FuGENE6 transfection reagent. At 24 hours after transfection, cells were starved in cysteine and methionine-free DMEM (Invitrogen) containing with 5% dialyzed FBS for 1 hour, then incubated for an additional 2 hours in cysteine and methionine-free DMEM containing 10% dialyzed FBS and 50 μCi/ml of Promix (Amersham). Labeled cells were then incubated in standard DMEM supplemented with 10% FBS and harvested at various time points. Immunoprecipitation was performed as described above.

Real-time quantitative PCR

MC3T3-E1-Tw1 cells (2×10^5 cells) were treated with BMP (600 ng) alone or the mixture of BMP (600 ng) and trichostatin (TSA, 330 nM; Sigma). At 24 hours after the treatment, total RNA was extracted from cells using RNeasy kits (Qiagen, Hilden, Germany) and digested with DNase I according to the manufacturer's instructions. Total RNA (5 μg) was reverse transcribed into cDNA using High Capacity cDNA Archive Kits (Applied Biosystems, Foster City, CA) and amplified by real-time quantitative PCR using an ABI PRISM 7700 Sequence Detection System (Applied Biosystems, Foster City, CA). Mixtures of probes and primer pairs specific for murine ALP, Runx2, osteopontin and GAPDH were purchased from Applied Biosystems (Foster City, CA). The concentration of target genes was determined using the comparative CT method (threshold cycle number at the cross-point between amplification plot and threshold) and values were normalized to an internal GAPDH control. Results are presented as mean ± s.d. from a representative experiment.

We wish to thank K. Miyazono for providing the 3GC2-Lux luciferase construct, BMPR-IB(QD) and TβR-I(TD), and Astellas Pharmaceutical Co. for providing rhBMP2. This work was supported by the Northern Osaka (Saito) Biomedical Knowledge-Based Cluster Creation Project, a Grant-in-Aid from the Ministry of Education,